Biomaterials 287 (2022) 121679

Contents lists available at ScienceDirect

Biomaterials

journal homepage: www.elsevier.com/locate/biomaterials

DAMP-modulating nanoparticle for successful pancreatic islet and stem cell transplantation

Soo Bin Jang [a,1], Sang-Man Jin [b,1], Hyung Shik Kim [a,1], Yong Yeon Jeong [c], Sang Jun Lee [a], Soojung Hahn [b,d], Hyemin Lee [b,d], Han Sin Lee [b], Jae Hyeon Kim [b,d,**], Dong Yun Lee [a,e,f,*]

[a] Department of Bioengineering, College of Engineering, Hanyang University, Seoul, 04763, Republic of Korea
[b] Division of Endocrinology and Metabolism, Department of Medicine, Samsung Medical Center, Sungkyunkwan University School of Medicine, Seoul, 06351, Republic of Korea
[c] Department of Radiology, Chonnam National University Hwasun Hospital, Chonnam National University Medical School, Hwasun, 58128, Republic of Korea
[d] Department of Health Sciences and Technology, SAIHST, Sungkyunkwan University, Seoul, 06355, Republic of Korea
[e] Institute of Nano Science & Technology (INST) & Institute for Bioengineering and Biopharmaceutical Research (IBBR), Hanyang University, Seoul, 04763, Republic of Korea
[f] Elixir Pharmatech Inc., Seoul, 04763, Republic of Korea

ARTICLE INFO

Keywords:
Damage-associated molecular pattern (DAMP)
Glycyrrhizin-chitosan conjugate
Superparamagnetic iron oxide nanoparticle
Inflammatory reaction
Magnetically guided transplantation

ABSTRACT

Cell therapy is targeted at many organs, but locally or systemically delivered cells are shortly able to survive resulting from the immune/inflammation reactions and irregular cell targeting. Here we explore the multimodal nanoparticle having anti-inflammation and magnetic guidance for successful cell transplantation. We design magnetic resonance (MR)-active glycyrrhizin-chitosan coated superparamagnetic iron oxide nanoparticle (SPIO@Chitosan-GL) to inhibit release of inflammatory damage-associated molecular pattern (DAMP) protein and to offer noninvasive monitoring after intrahepatic transplantation of pancreatic islets and mesenchymal stem cell (MSC) spheroids. Intracellular delivered SPIO@Chitosan-GL is not cytotoxic to pancreatic islets and MSC spheroids and attenuate DAMP release from them. Also, therapeutic cells labeled with SPIO@Chitosan-GL are magnetically localized to the intended lobe of liver during transplantation procedure. If necessary, partial hepatectomy can be performed to remove the localized therapeutic cells for protection of the remaining liver lobes from systemic inflammation. Therapeutically, the cells selectively localized in the liver can treat blood glucose in diabetic mice to normal levels with DAMP modulation, and are visualized using in vivo MR imaging for over 4 weeks. Collectively, DAMP-modulating SPIO@Chitosan-GL can be used in multimodal nanomedince for attenuating the inflammation reaction by transplanted cells and for noninvasively long-term monitoring of transplanted cells.

1. Introduction

Cytotherapy (also called cell transplantation or cell delivery) is transplantation of viable stem cells or mature (differentiated) cells into a patient to exert a therapeutic effect through the secretion of the relevant therapeutic factors [1]. Therefore, cytotherapy is targeted at many organs by several strategies. However, locally or systemically delivered cells are usually able to survive for relatively short periods of time (days-weeks) resulting from the host's immune reactions and irregular cell targeting.

Insulin-secreting pancreatic islet transplantation is currently the only promising strategy to simultaneously achieve normal blood glucose level in patients with type I diabetes mellitus, which is complicated by impaired awareness of hypoglycemia [2–4]. Clinically, the donated islets cells are intrahepatically transplanted in the liver of diabetic patients. However, the substantial loss of transplanted islet cell mass is primarily attributable to the host's immune responses and the instant blood-mediated inflammatory reactions (IBMIR). Importantly, in severe

* Corresponding author. Department of Bioengineering, College of Engineering, Hanyang University, Seoul, 04763, Republic of Korea.
** Corresponding author. Division of Endocrinology and Metabolism, Department of Medicine, Samsung Medical Center, Sungkyunkwan University School of Medicine, Seoul, 06351, Republic of Korea.
E-mail addresses: jaehyeon@skku.edu (J.H. Kim), dongyunlee@hanyang.ac.kr (D.Y. Lee).
[1] These authors contributed equally (co-first authors).

https://doi.org/10.1016/j.biomaterials.2022.121679
Received 30 January 2022; Received in revised form 29 June 2022; Accepted 9 July 2022
Available online 12 July 2022

cases of islet graft rejection, the antigenic islets should be removed rapidly to protect the liver organ from the immune reaction and inflammation. However, the transplanted islets spread widely throughout the liver, making it impossible to remove them from the liver. On the other hand, High-mobility group box 1 (HMGB1) is a non-chromosomal DNA-binding nuclear factor protein that is present in almost all eukaryotic cells, but is more abundant in islets [5]. During immune response and inflammation, unavoidable damage to the islet causes the release of HMGB1 protein into the extracellular space. Extracellular HMGB1 plays a key role in the potent activation of innate immunity and proinflammatory cytokine production [6–8]. Therefore, multifunctional remedies to control HMGB1 action will provide a breakthrough for successful clinical cell transplantation.

Glycyrrhizin (GL), clinically used as a treatment for hepatitis in Japan, is a well-known inhibitor of HMGB1, which directly binds to two shallow concave surfaces formed by the two arms of both HMG boxes [9]. In addition, GL attenuate the inflammatory response through lowing the activity of 11β-Hydroxysteroid dehydrogenase (11β-HSD) in cell [10–12]. Therefore, GL would enhance the protective effect on the therapeutic cells. Meanwhile, superparamagnetic iron oxide (SPIO) nanoparticle is a safe and well-proven method that has been used in clinical magnetic resonance imaging (MRI) for decades [13–15]. Furthermore, SPIO nanoparticles would be a potential agent for magnetic guidance of therapeutic cells to injured organs [16–19]. Therefore, here we developed Chitosan-GL-coated SPIO nanoparticle (called SPIO@Chitosan-GL). The amine group of water-soluble glycol chitosan was chemically conjugated with aldehyde group of the oxidized GL, which was further treated with as-prepared SPIO nanoparticle requiring sonication and heating method [20,21]. Therefore, this MRI-active SPIO@Chitosan-GL nanoparticle would be multimodal nanomedicine with anti-inflammation and magnetic guidance for successful therapeutic cell transplantation (Fig. 1).

To prove this hypothesis, we investigated the benefit of MRI-active SPIO@Chitosan-GL treatment on islets and/or adjuvant mesenchymal stem cell (MSC) spheroids in intrahepatic cell transplantation. First, we internalized the synthesized SPIO@Chitosan-GL nanoparticles into islets and MSC spheroids. We then tested the feasibility of magnetic guidance of the labeled therapeutic cells, and their ability to attenuate HMGB1

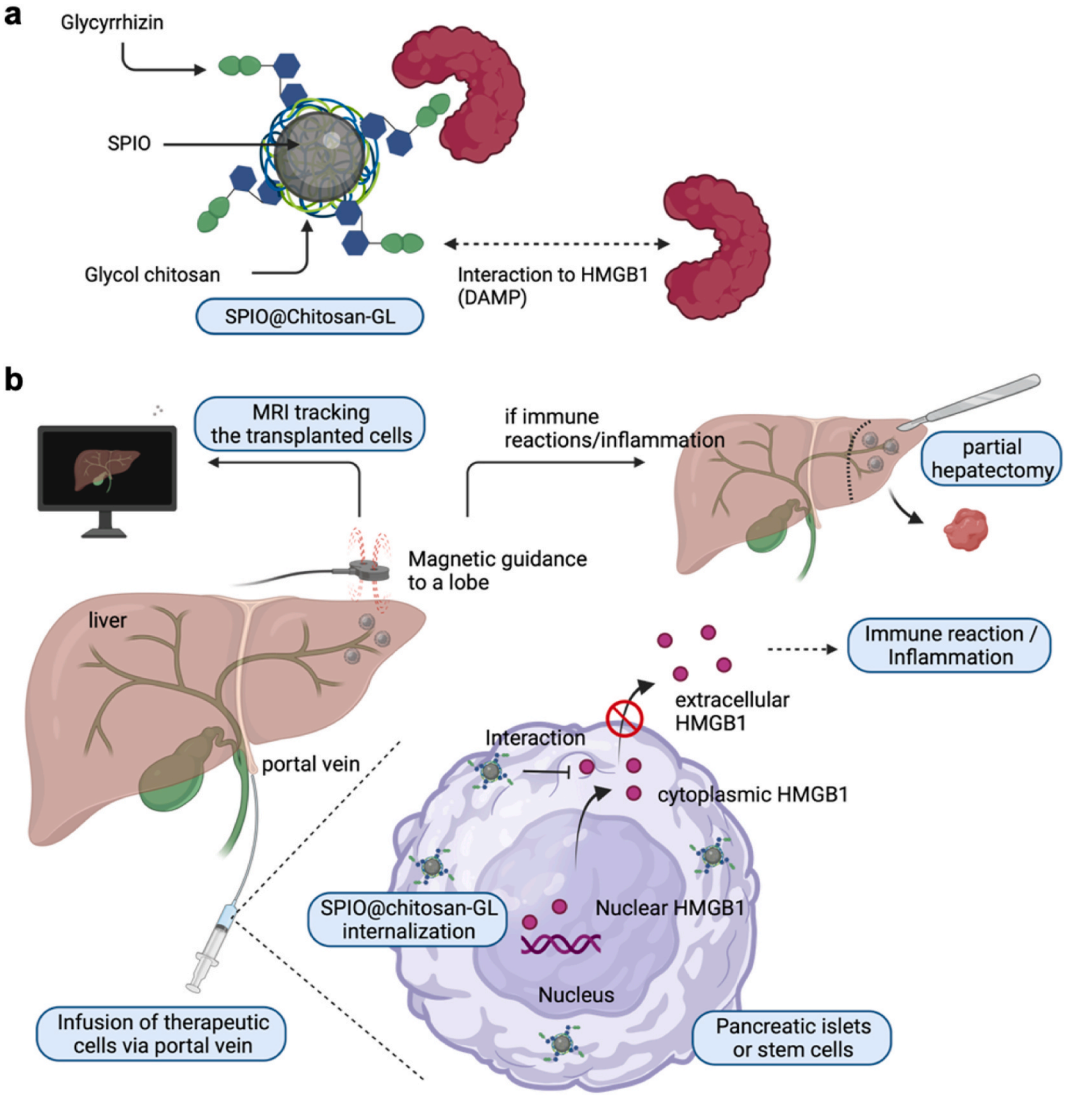

Fig. 1. Magnetic nanoparticle with glycyrrhizin-chitosan conjugate (Chitosan-GL) and its application. **(a)** Schematic structure of superparamagnetic iron oxide nanoparticle coated with chitosan-GL (SPIO@Chitosan-GL) for binding the HMGB1, a DAMP protein. **(b)** Application of SPIO@chitosan-GL for successful cell transplantation. After internalization of SPIO@Chitosan-GL into therapeutic cells (pancreatic islets and stem cells), they could be intraportally transplanted into the liver under the magnetic guidance. In addition, the internalized SPIO@Chitosan-GL could reduce the inflammation reaction of transplanted cells, and they could be visualized by using MR imaging for a long time. If immune reaction/inflammation is occurred at the specific lobe, the transplanted cells could be eliminated by partial hepatectomy.

release in the labeled therapeutic cells. Next, the labeled therapeutic cells were intrahepatically transplanted into specific lobe of liver organ of diabetic mice under the magnetic guidance. Finally, glycemic outcome for their therapeutic effect and persistence of SPIO@Chitosan-GL nanoparticle in them were evaluated.

2. Results and discussion

2.1. Charaterization of MRI-active SPIO@Chitosan-GL nanoparticle

To prepare MRI-active SPIO@Chitosan-GL nanoparticle, the glycyrrhizin-chitosan conjugate (Chitosan-GL) was synthesized via the linkage between amine group of chitosan and aldehyde group of the oxidized glycyrrhizin (oGL) (Fig. S1 and Fig. S2). The linkage of glycyrrhizin to glycol chitosan was confirmed by proton nuclear magnetic

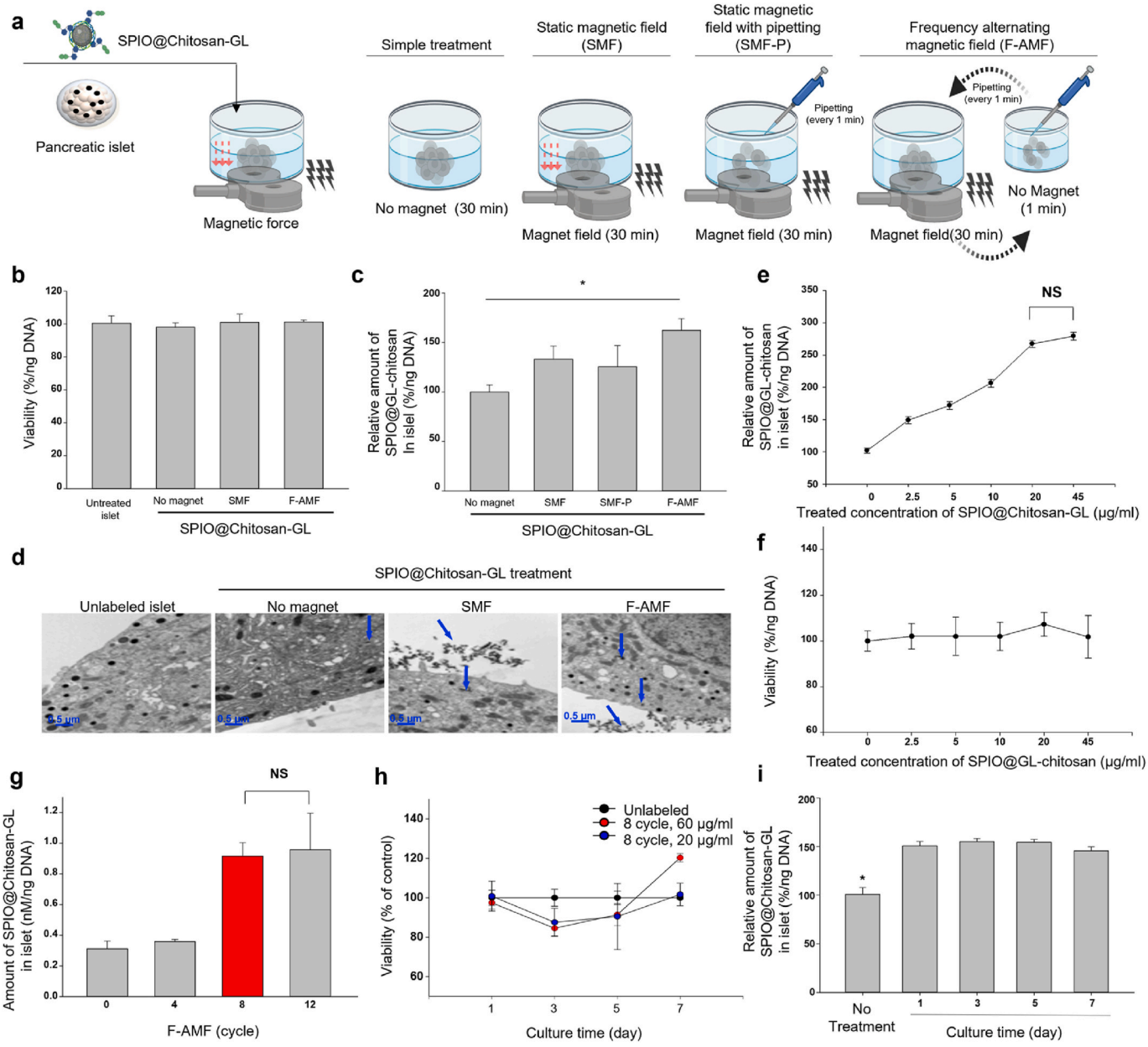

Fig. 2. Optimization of SPIO@Chitosan-GL internalization into pancreatic islets. (**a**) Schematic strategy for internalization of SPIO@Chitosan-GL. (**b**) The cell viability of pancreatic islets labeled with four experimental strategies: unlabeled islets without SPIO@Chitosan-GL, static magnetic field (SMF), Frequency-alternating magnetic field (F-AMF). Data were expressed as mean ± s.e.m (n = 5). (**c**) Relative amount of SPIO@Chitosan-GL labeled with four experimental strategies. Data were expressed as mean ± s.e.m (n = 5). *$P < 0.05$. (**d**) TEM image of islets labeled with four experimental strategies. (**e**) Relative amount of SPIO@Chitosan-GL in pancreatic islet labeled with F-AMF strategy according to different treatment concentration of SPIO@Chitosan-GL. Data were expressed as mean ± s.e.m (n = 5). NS: not significant. (**f**) The viability of pancreatic islet labeled with F-AMF strategy according to different treatment concentration of SPIO@Chitosan-GL. Data were expressed as mean ± s.e.m (n = 5). (**g**) Relative amount of SPIO@Chitosan-GL in pancreatic islet labeled with F-AMF strategy according to different repeat times (cycle). Data were expressed as mean ± s.e.m (n = 5). NS: not significant. (**h**) The viability of pancreatic islet labeled with SPIO@Chitosan-GL (20 or 60 μg/ml) by using F-AMF strategy (8 cycles) during different cultivation time. Data were expressed as mean ± s.e.m (n = 5). (**i**) Relative amount of SPIO@Chitosan-GL in pancreatic islet labeled with F-AMF strategy according to different cultivation time (day). Data were expressed as mean ± s.e.m (n = 5).

resonance (^{1}H NMR) spectroscopy (Fig. S3~S6). The single peak at δ 5.67 was attributed to the protons of olefinic bond (-(C═O)–CH═C-) in GL. The peaks at δ 3.61–3.71 were attributed to the protons from the chitosan backbone and the protons from the glucuronic acids in GL. The peak at δ 2.73 came from the protons of C-2 in secondary amine linkage (acetyl group or GL). Thus, Chitosan-GL conjugate was successfully synthesized. Then the Chitosan-GL conjugate was treated on SPIO nanoparticles prepared by co-precipitation of Fe^{3+} and Fe^{2+} salts in basic aqueous solution to prepare MRI-active SPIO@Chitosan-GL nanoparticle (Fig. S7a). The typical surface potential and size of bare SPIO (no coating with Chitosan-GL) and SPIO@Chitosan-GL was measured with a zeta sizer (Nano ZS, Melvern, UK), and the morphology of SPIO@Chitosan-GL was analyzed with transmission electron microscope (TEM). The surface potential of SPIO@Chitosan-GL was 0.2 ± 0.1 mV in PBS at pH 7.4, whereas that of bare SPIO was −0.1 ± 0.2 mV (Fig. S7c). The both particle size and hydrodynamic diameter of SPIO@Chitosan-GL (8.4 ± 0.3 nm and 136 ± 3.6 nm, respectively) was smaller than bare SPIO nanoparticle (14.9 ± 0.4 nm and 175 ± 2.7 nm, respectively) (Figs. S7b and S7c). Based on these findings, Chitosan-GL that coated on the surface of SPIO nanoparticle inhibits the overgrowth of nanoparticle and stabilize the interface where nanoparticle interact with medium. Moreover, the polydispersity index (PDI) of SPIO@Chitosan-GL was maintained below 0.2 value after 2 weeks of storage, demonstrating stability against aggregation and nanoparticles of uniform-size. To quantify Chitosan-GL amounts in SPIO@Chitosan-GL, a 70% nitric oxide solution was added to the lyophilized SPIO@Chitosan-GL and heated to 180 °C for 2 h to remove organic compounds. Then, the iron amount of the samples was measured with inductively coupled plasma-mass spectrometry (ICP-MS). Therefore, the amounts of Chitosan-GL in SPIO@Chitosan-GL was obtained by subtracting the iron contents from the pre-measured mass of the lyophilized SPIO@Chitosan-GL (Fig. S7d). As a result, the average amount of Chitosan-GL out of 52.0 mg of SPIO@Chitosan-GL was 18.4 ± 0.3 mg (0.35 mg of Chitosan-GL per 1 mg of SPIO@Chitosan-GL). Unfortunately, the exact binding ratio between glycol chitosan (GC) and glycyrrhizin in the Chitosan-GL conjugate is not available to be calculated. This is because the molecular weight of GC ranges from 20 to 250 kDa with the degree of deacetylation from 60 to 82.7%.

2.2. Optimization of intracellular uptake of SPIO@Chitosan-GL into pancreatic islets

To optimize intracellular uptake of SPIO@Chitosan-GL into the isolated pancreatic islets, various concentrations of SPIO@Chitosan-GL were treated to pancreatic islets. To this end, we first set for different strategies with different treatment times and reaction time: (a) simple treatment without magnet, (b) static magnetic field (SMF), (c) static magnetic field with gentle pipetting (SMF-P), and (d) frequency alternating magnetic field (F-AMF); 1 cycle = first static magnetic field for 1 min and then no magnetic field with gentle pipetting for 1 min (Fig. 2a). Regardless of the conditions used for intracellular uptake process, the viability of the labeled pancreatic islets was not affected (Fig. 2b). Among the four conditions, the highest iron content was achieved by F-AMF strategy (Fig. 2c). Representative TEM images of the internalized SPIO@Chitosan-GL nanoparticles were shown in Fig. 2d (blue arrow). In the case of F-AMF strategy, SPIO@Chitosan-GL nanoparticles were highly internalized into the islet cells. Furthermore, when SPIO@Chitosan-GL was treated up to 45 μg/ml with F-AMF strategy, the relative amount of intracellular SPIO@Chitosan-GL reached plateau at 20 and 45 μg/ml without changes in the viability of islet (Fig. 2e and f). Next, when F-AMF was repeated up to 12 cycles, the amount of SPIO@Chitosan-GL nanoparticles internalized into the islet cells reached plateau at 8 and 12 cycles (Fig. 2g). The intracellular SPIO@Chitosan-GL nanoparticles did not affect the viability of pancreatic islet for 7 days (Fig. 2h). In addition, intracellular SPIO@Chitosan-GL nanoparticles maintained in the islets, suggesting that no damage of islet viability was not occurred by the loss of the intracellular SPIO@Chitosan-GL nanoparticles (Fig. 2i). Collectively, with the optimized intracellular uptake strategy, *i.e.*, F-AMF strategy, pancreatic islets were stably labeled with SPIO@Chitosan-GL nanoparticles. SMF strategy was also constant field with a frequency of 0 Hz, which was no change in intensity or direction over time. Therefore, SPIO@Chitosan-GL nanoparticles were not largely internalized into the islet when applied with SMF strategy. However, F-AMF strategy below the surface of the cell culture plate has a regular frequency, which could generate oscillation of SPIO@Chitosan-GL nanoparticles. Accordingly, F-AMF could strongly pull SPIO@Chitosan-GL nanoparticles into contact with the islet cell membrane and then SPIO@Chitosan-GL nanoparticles were largely internalized into the islet cells with high efficiency in the absence of damage. On the other hand, it is well known that the coating of SPIO with non-magnetic polymers like polysaccharide or its derivative such as our glycol chitosan leads to a decrease in magnetization as compared with bare SPIO [22]. Nevertheless, we showed that F-AMF strategy could be suitable to enhance the internalization of SPIO@Chitosan-GL nanoparticles. Collectively, based on these findings, the intracellular uptake strategy of SPIO@Chitosan-GL into islets were optimized with F-AMF strategy.

2.3. Functionality of pancreatic islets labeled with SPIO@Chitosan-GL nanoparticle

It has been reported that magnetic forces (strength of a magnetic field or magnetic flux density) greater than 2–3 T (Tesla) can cause short-term effects such as dizziness, irregular movement, and nausea in patients due to generation of small electrical current [23–25]. In our study, a magnetic force with 0.2 T (or 2000 G) was used for the internalization of SPIO@Chitosan-GL nanoparticles. Therefore, the F-AMF strategy may not have adverse effects on islets. To determine if the F-AMF strategy to internalize SPIO@Chitosan-GL nanoparticles could affect islets, we metabolically evaluated the viability and function of islets. The viability of islets labeled with SPIO@Chitosan-GL was not impaired, which was assessed via fluorescent dye staining (Fig. 3a and b). Mitochondrial markers, essentially one of the most reliable predictors of islet function, are important for assessing islet health [26,27]. No metabolic change in the cytosolic ADP/ATP ratio was measured (Fig. 3c). Therefore, using F-AMF strategy, metabolism of islets labeled with SPIO@Chitosan-GL nanoparticles was not affected. For further evaluation of SPIO@Chitosan-GL-labeled islet function, the amount of insulin secreted from them during static incubation at low and high glucose concentration was measured. The secretion patterns of insulin protein and the stimulation index (SI) values of glucose were similar in all experimental groups (Fig. 3d and e). Overall, it was confirmed that internalization of SPIO@Chitosan-GL did not affect the viability and function of islets. To assess whether SPIO@Chitosan-GL attenuated the release of HMGB1 in islets, islets were damaged by treatment of streptozotocin (STZ; 1.5 mM) for 2 h, which was confirmed by AO/PI fluorescence staining (Fig. 3f). Thereafter, the level of HMGB1 in the medium was immediately investigated. In the unlabeled or bare SPIO-labeled islets, the release of HMGB1 was significantly increased by STZ injury (Fig. 3g). However, the release of HMGB1 from SPIO@Chitosan-GL-labeled islets was not increased even though the treated STZ damaged islets. The mechanisms by which cells release HMGB1 into the extracellular environment are either passive or active [28]. HMGB1 is passively released into extracellular space from damaged cells, and then it acts as a cytokine-like-factor that recruits immune cells by binding to receptors such as Toll-like receptors (TLRs) as well as receptors for advanced glycation end products (RAGE). Then, the activated immune cells actively released HMGB1 again. Therefore, blocking initiation of HMGB1-derived immune response is considered an important strategy to prevent exacerbation of cellular damage. From these results, we found that SPIO@Chitosan-GL nanoparticles introduced into cells could functionally inhibit the passive release of HMGB1

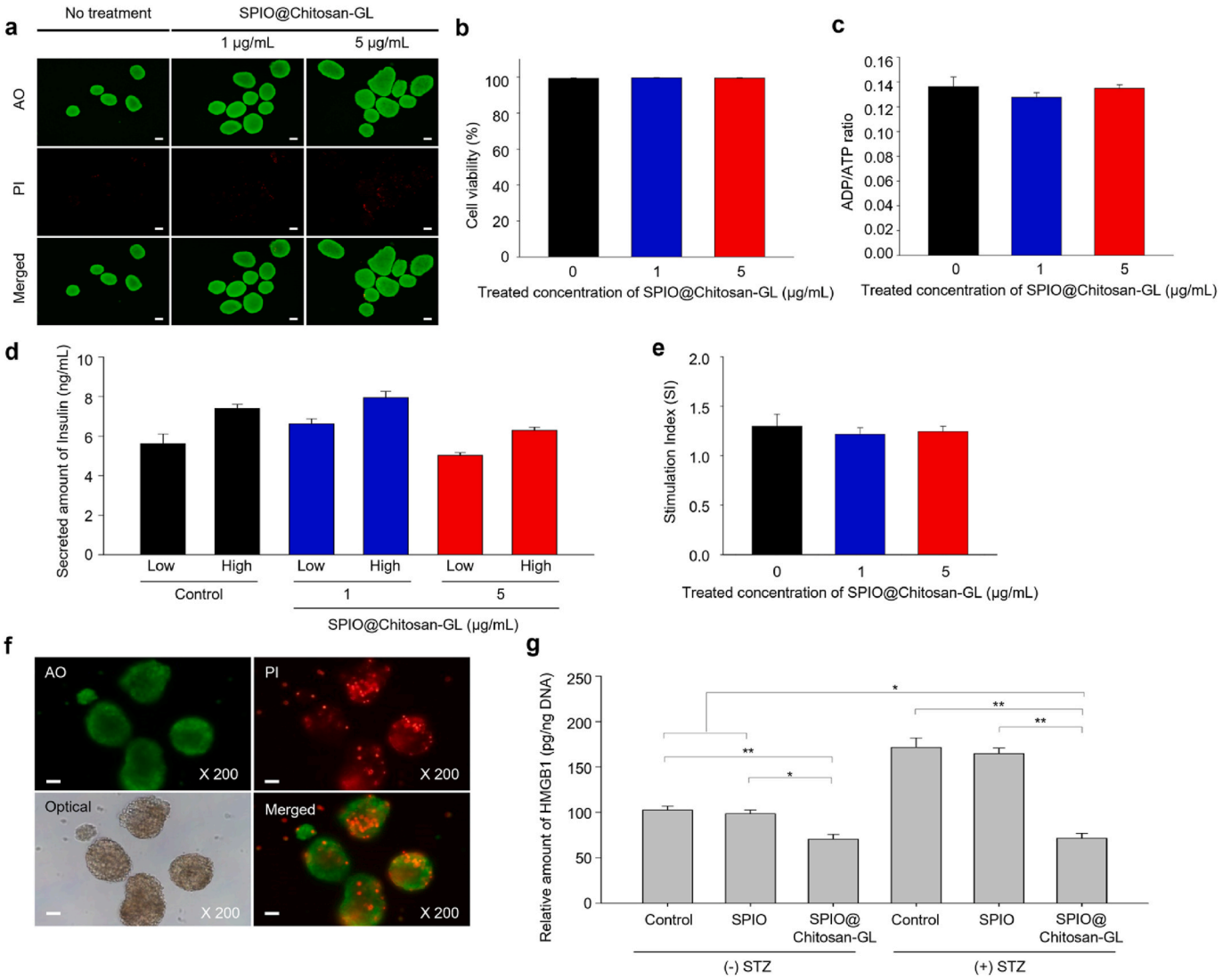

Fig. 3. Effect of SPIO@Chitosan-GL internalized into the pancreatic islets. (**a**) Fluorescent acridine orange (AO)/propidium iodide (PI) stain of unlabeled islets (control) and SPIO@Chitosan-GL-labeled islets. Scale bar: 100 μm. (**b**) The viability of unlabeled islets (control) and SPIO@Chitosan-GL-labeled islets. Data were expressed as mean ± s.e.m (n = 5). (**c**) The changes in ADP/ATP ratio of unlabeled islets (control) and SPIO@Chitosan-GL-labeled islets. Data were expressed as mean ± s.e.m (n = 5). (**d**) Glucose-stimulated insulin secretion (GSIS) assay to unlabeled islets (control) and SPIO@Chitosan-GL-labeled islets. Data were expressed as mean ± s.e.m (n = 5). (**e**) Stimulation index (SI) value to unlabeled islets (control) and SPIO@Chitosan-GL-labeled islets after GSIS assay. Data were expressed as mean ± s.e.m (n = 5). (**f**) Fluorescent AO/PI stain of unlabeled islets treated with streptozotocin (STZ, 1.5 mM) for 2 h. Scale bar: 100 μm. (**g**) Secreted amount of HMGB1 from unlabeled islets (control) and SPIO@Chitosan-GL-labeled islets without or with treatment of streptozotocin (STZ, 1.5 mM) for 2 h. Data were expressed as mean ± s.e.m (n = 5). $*P < 0.05$, $**P < 0.01$. (For interpretation of the references to color in this figure legend, the reader is referred to the Web version of this article.)

after cell damage, which is the starting point of immune response after cell injury. Moreover, it has been reported that iron oxide nanoparticle such as SPIO are aggregated in the cytoplasmic fraction of islets due to their ferrimagnetic properties to prevent exocytosis for a long period of time [29]. In the case of SPIO@Chitosan-GL, it would have been further improved the islets through binding GL to HMGB1 for inhibition of passive release of HMGB1 from islets.

2.4. *Magnetic guidance of SPIO@Chitosan-GL-labeled pancreatic islets during the intrahepatic transplantation*

For MR imaging, the magnetic property of SPIO@Chitosan-GL nanoparticle was characterized with T2*-weighted MR image. To this end, T2*-weighted images were obtained by using *in vitro* phantom of agar gel with different concentration of SPIO@Chitosan-GL nanoparticle. As a result, SPIO@Chitosan-GL nanoparticle demonstrated a log-linear dependency of the 1/T2* (T2 relaxation rate, a measure of T2* value within the regions of interest (ROI) values on the SPIO@Chitosan-GL concentration (Fig. S8). T2*-weighted MR images of SPIO@Chitosan-GL nanoparticle with more than 8.3 μg/ml were blurred, suggesting that low concentration of SPIO@Chitosan-GL is possible enough to image pancreatic islets. After that, pancreatic islets labeled with 5 μg/ml of SPIO@Chitosan-GL were intrahepatically transplanted to visualize them in the whole liver. In the absence of magnetic guidance, the hypointense spots representing SPIO@Chitosan-GL-labeled islets were distributed throughout the liver (Fig. 4a). Under magnetic guidance, however, they were highly localized into the median lobe of liver. To clearly analyze the distribution of them in each lobe of liver organ, the dissociated lobes were analyzed with *in vitro T2*-weighted MRI phantom (Fig. 4b and Fig. S9). The islets were specifically localized in the median (M1 & M2) lobe of liver via magnetic guidance. To quantify their hypointensity in agar gel phantom, we analyzed the T2 relaxation time of each lobe

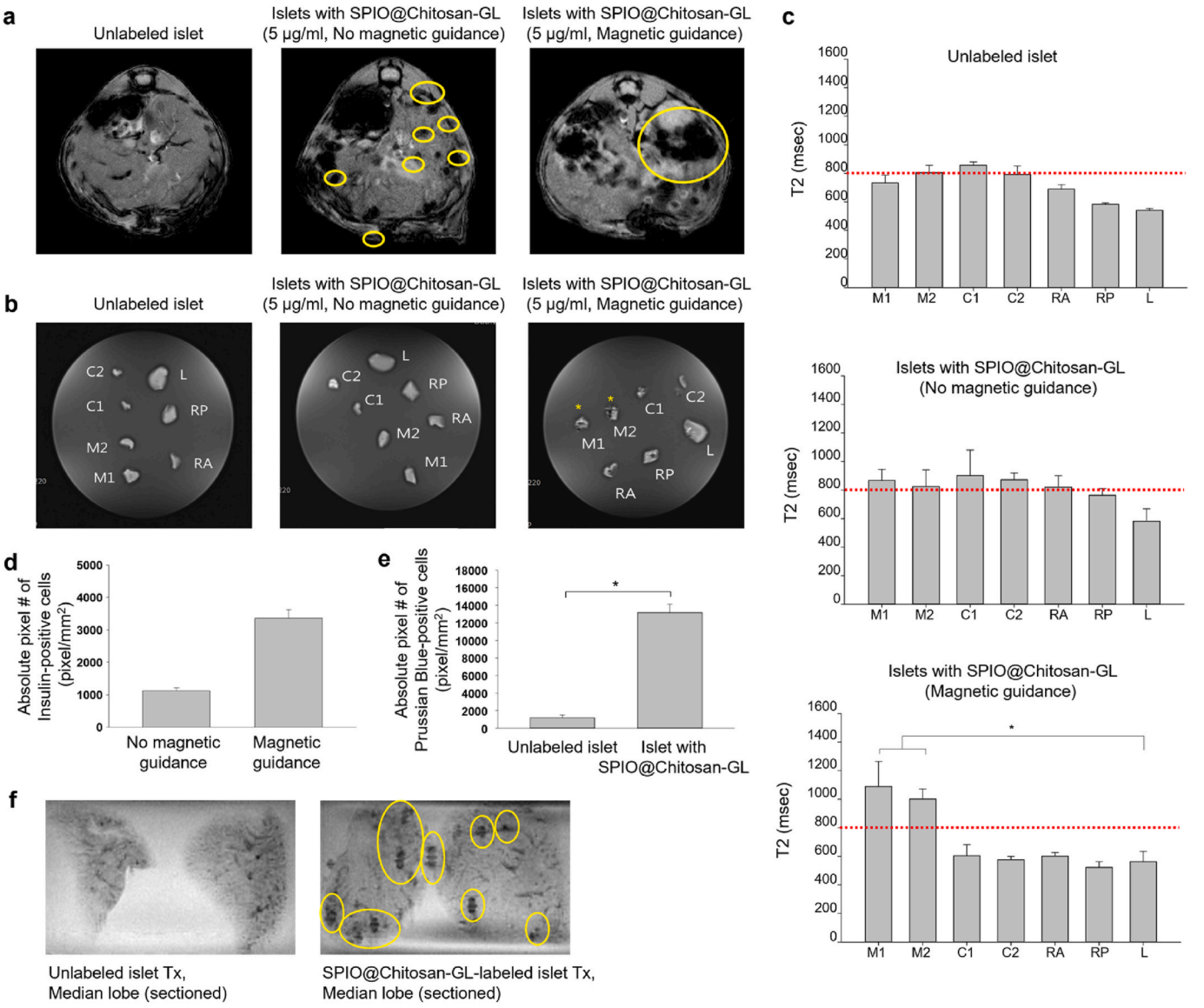

Fig. 4. *In vivo* and *in vitro* MR image analysis of SPIO@Chitosan-GL-labeled islets after intraportal transplantation. (**a**) *T2*-weighted MR image of unlabeled islet (control) and SPIO@Chitosan-GL-labeled islets after intraportal transplantation without or with magnetic guidance. Yellow circle: SPIO@Chitosan-GL-labeled islets. (**b**) *In vitro T2*-weighted MR phantom image of each lobe of liver organ dissociated from the recipient after intraportal transplantation without or with magnetic guidance. C1 and C2: Caudate lobe, M1 and M2: Median lobe, L: Left lobe, RA: Right Anterior, RP: Right Posterior. (**c**) T2 relaxation time of each lobe of liver organ after *In vitro T2*-weighted MR phantom analysis from Fig. 4b. Red dash line: T2 relaxation time or liver organ on average. $^*P < 0.05$. (**d**) Absolute pixel number of insulin-positive cells from the whole sections of median lobe by using Image-J software. Data were expressed as mean ± s.e.m (n = 5). (**e**) Absolute pixel number of Prussian Blue-positive cells from the whole sections of median lobe by using Image-J software. Data were expressed as mean ± s.e.m (n = 5). $^*P < 0.05$. (**f**) *In vitro* MR phantom analysis of agarose gel phantom with pancreatic islets without or with SPIO@Chitosan-GL labeling. Yellow circle: MR-positive islets. (For interpretation of the references to color in this figure legend, the reader is referred to the Web version of this article.)

(Fig. 4c). T2 relaxation time due to magnetic guidance was significantly longer in the median (M1 & M2) lobe than in other lobes. To confirm the presence of SPIO@Chitosan-GL in the median lobe, all sectioned slices of the whole median lobe were stained with anti-insulin (for insulin-secreting islet stain) and prussian blue dye (for SPIO@Chitosan-GL stain) (Fig. 4d and e, and Fig. S10). In addition, the sectioned slices of the median lobe were visualized with *in vitro* MRI phantom analysis (Fig. 4f). From these findings, we found that SPIO@Chitosan-GL-labeled pancreatic islets could be intrahepatically transplanted into the target median lobe of liver organ through magnetic guidance.

2.5. Internalization of SPIO@Chitosan-GL into murine pancreatic mesenchymal stem cell (MSC)

Because of their immunomodulatory properties as well as survival and angiogenesis-promoting properties, co-transplantation of islets and human mesenchymal stem cell (MSC) in portal sinusoids has been an active area of investigation [30–32]. To the best of our knowledge, however, translational potential of this approach in clinical allogeneic islet transplantation has not been tested in diabetic patients. One of the important issues is the instant blood mediated inflammatory reaction (IBMIR) induced by intrahepatically infused MSCs, potentially leading to immune-mediated clearance of therapeutic cells and portal vein thrombosis [33]. Recently, we observed that the thrombogenic properties of MSCs were weakened by forming the spheroids of them instead of

single cells [34]. To further control the inflammation of MSCs in the liver organ, here we first demonstrated that internalization of SPIO@Chitosan-GL into murine pancreatic MSC spheroids could attenuate the release of HMGB1 and resultant conversion of complement factor C3 into C3a in the bloodstream, an effector of the complement system, with functioning immune cells' activation. To this end, SPIO@Chitosan-GL nanoparticles were treated to the cultured MSCs with frequency alternating magnetic field (F-AMF), and then the SPIO@Chitosan-GL-labeled MSCs were aggregated by conventional hanging-drop method (Fig. 5a). SPIO@Chitosan-GL nanoparticles were dose-dependently internalized in the MSCs, which was quantified by the iron assay (Fig. 5b and c). The viability of SPIO@Chitosan-GL-labeled MSCs was not impaired for a day when SPIO@Chitosan-GL was treated up to 80 μg/ml (Fig. 5d). However, when the SPIO@Chitosan-GL-labeled MSCs were cultured for 7 days, the viability of them treated with more than 20 μg/ml was damaged. Conversely, it can be confirmed that no cytotoxicity was found until the 7th day at a treatment concentration of 20 μg/ml or less. To evaluate whether SPIO@Chitosan-GL affect the proliferation of MSCs, the proliferation rate of SPIO@Chitosan-GL-labeled MSCs was measured for 7 day. The proliferation of SPIO@Chitosan-GL-labeled MSCs was similar to that of unlabeled MSCs (Fig. S11), which was similar to the average doubling time (2–3 days) of MSCs [35]. In addition, when MSCs were treated with less than 20 μg/ml of SPIO@Chitosan-GL, the MSC spheroid formed with all initial cell numbers using the hanging-drop method (Fig. 5e and f). To visualize the internalized SPIO@Chitosan-GL at up to 20 μg/ml, the SPIO@Chitosan-GL-internalized MSCs were stained with prussian blue dye, suggesting that the low concentration of SPIO@Chitosan-GL (20 μg/mL or less) could be sufficiently internalized into MSCs (Fig. 5g). Based on these findings, the concentration of SPIO@Chitosan-GL for MSC labeling was optimized to 20 μg/ml.

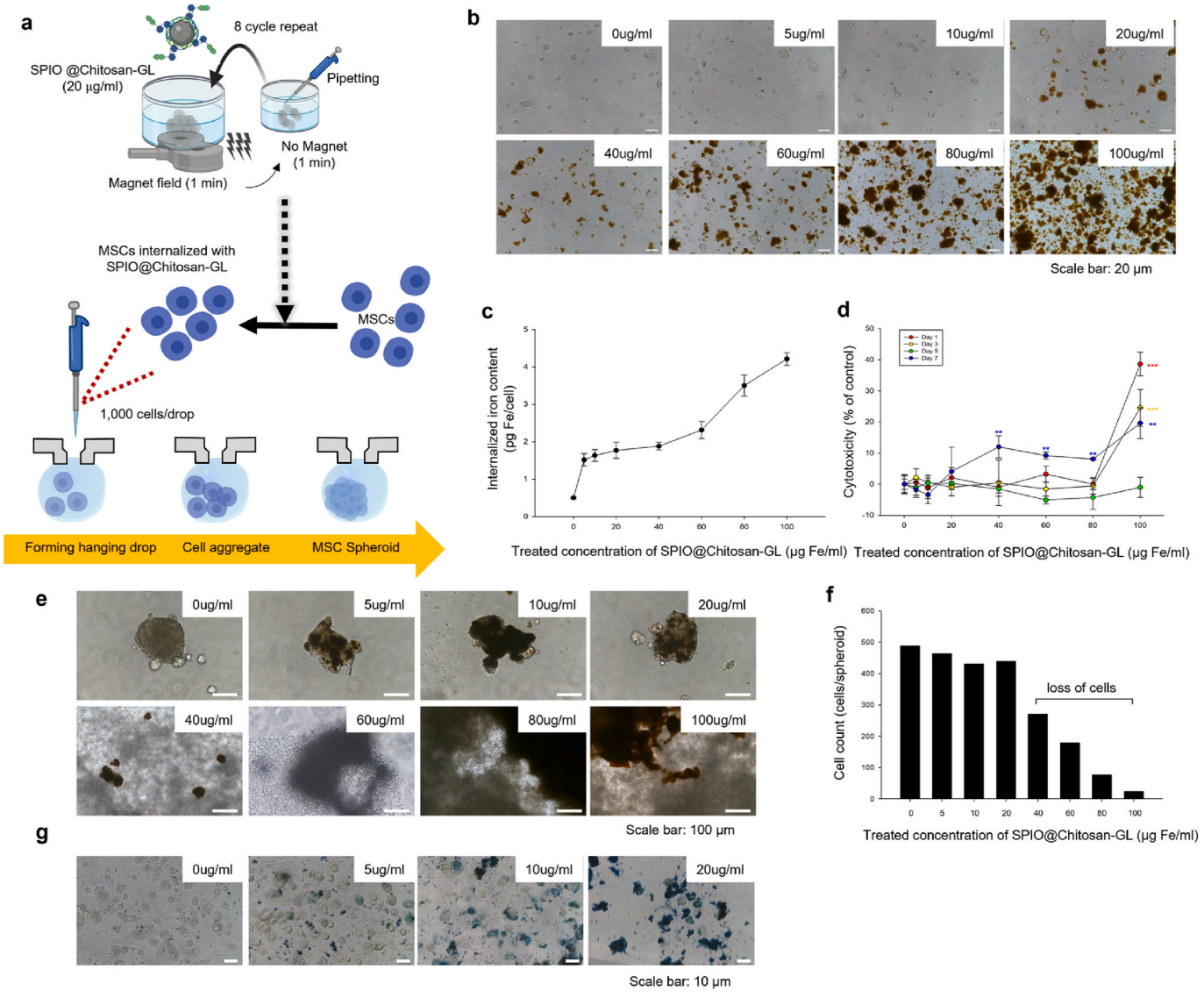

Fig. 5. Optimization of SPIO@Chitosan-GL labeling to mesenchymal stem cells (MSC). (**a**) Spheroid formation of MSC labeled with SPIO@Chitosan-GL. (**b**) Optical image of MSCs after treatment with different concentration of SPIO@Chitosan-GL nanoparticle. Scale bar: 100 μm**.** (**c**) Internalized amount of SPIO@Chitosan-GL into MSCs after treatment with different concentration of SPIO@Chitosan-GL nanoparticle. Data were expressed as mean ± s.e.m (n = 5). (**d**) Cytotoxicity of SPIO@Chitosan-GL nanoparticle to MSCs during cultivation time after treatment with different concentration of SPIO@Chitosan-GL nanoparticle. Data were expressed as mean ± s.e.m (n = 5). $^{**}P < 0.01$. $^{***}P < 0.001$. (**e**) Spheroid formation of MSCs labeled with different concentration of SPIO@Chitosan-GL. Scale bar: 100 μm. (**f**) Aggregated cell numbers per each MSC spheroid that were formed with MSCs labeled with different concentration of SPIO@Chitosan-GL (n = 1). (**g**) Prussian Blue stain image of MSC spheroid that were formed with MSCs labeled with different concentration of SPIO@Chitosan-GL. Scale bar: 10 μm. (For interpretation of the references to color in this figure legend, the reader is referred to the Web version of this article.)

2.6. Magnetic guidance of SPIO@Chitosan-GL-labeled MSC spheroids during the intrahepatic transplantation

Next, we evaluated whether MSC spheroids labeled with SPIO@Chitosan-GL could be magnetically guided during the intrahepatic transplantation. As control, SPIO@Chitosan-GL-labeled MSC spheroids were also transplanted without magnetic field (negative control) or with surgical vascular clamp (positive control). After transplantation of them in the liver through the portal vein, the liver organ was scanned with *T2*-weighed MR scanner. SPIO@Chitosan-GL-labeled MSC spheroids were well magnetically guided to the target median lobe of liver organ, which were similar to positive control (yellow circle, Fig. S12). However, the simply infused MSC spheroids were not clearly detected in the intended lobe because of the lack of magnetic guidance. These results suggested that MSC spheroids labeled with SPIO@Chitosan-GL could be well guided by magnetic targeting effect. However, the MR images of the liver with SPIO@Chitosan-GL-labeled MSC spheroids were severely blurred, meaning that 20 μg/ml of SPIO@Chitosan-GL was still high concentration.

On the other hand, we confirmed the persistence of SPIO@Chitosan-GL MSC spheroids in the recipient liver tissue by iron staining, which was obtained three weeks after the allogeneic intraportal transplantation of SPIO@Chitosan-GL MSC spheroids alone (Fig. S13). MSC spheroid were stained with green fluorescent protein (GFP)-antibody, as murine pancreatic MSCs in this study were isolated from male GFP-transgenic C57BL/6J mice. As a result, extensive uptake of

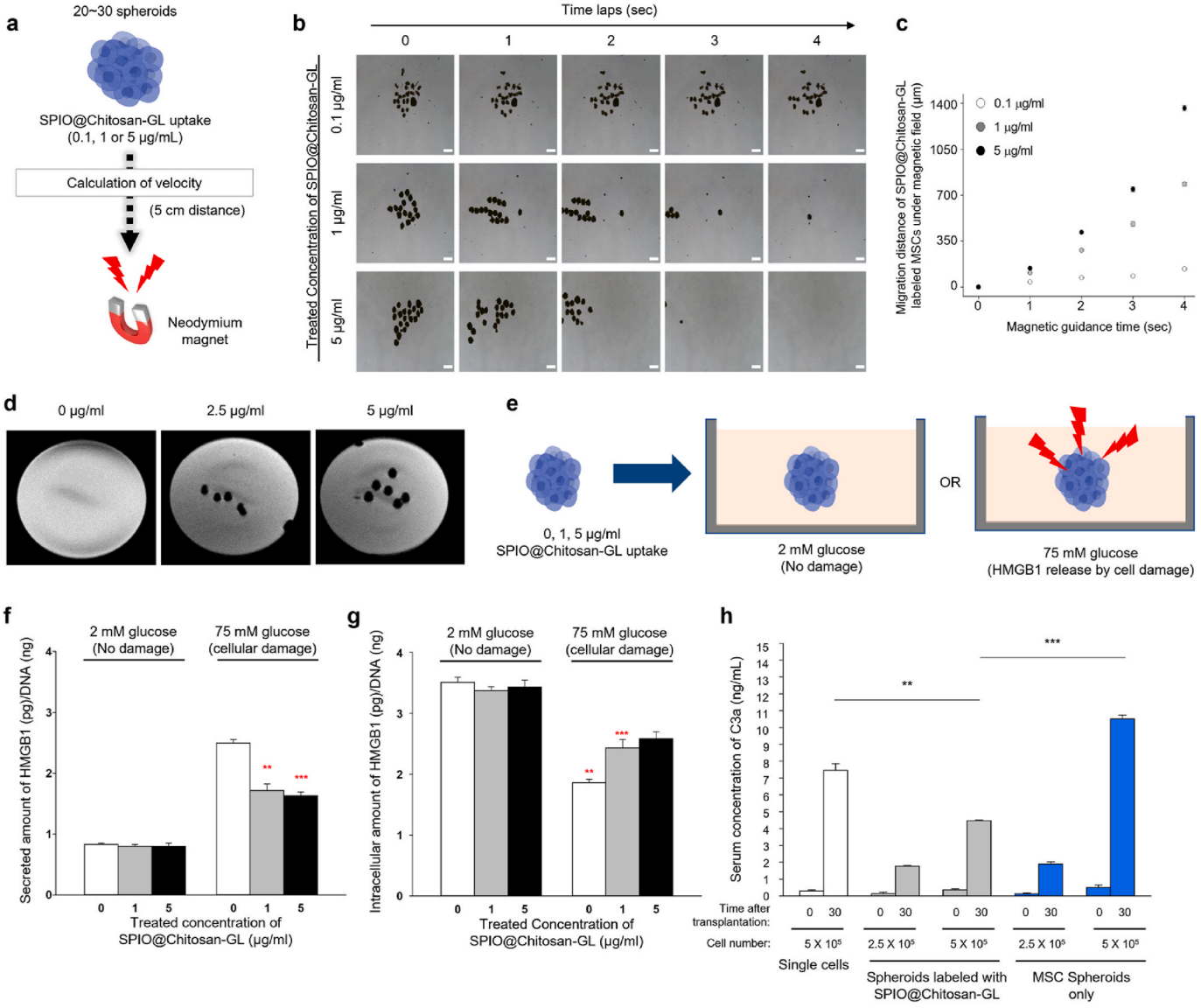

Fig. 6. Effect of SPIO@Chitosan-GL internalized into the MSC spheroid. **(a)** MSC spheroids labeled with different concentration of SPIO@Chitosan-GL. **(b)** The images of moving MSC spheroids labeled with different concentration of SPIO@Chitosan-GL. Scale bar: 20 μm. **(c)** Migration distance of SPIO@Chitosan-GL labeled MSCs spheroid under magnetic field. **(d)** *In vitro T2*-weighted MRI phantom analysis of MSC spheroids labeled with each concentration of SPIO@Chitosan-GL. **(e)** Experimental scheme for cellular damage to MSC spheroids during cultivation with high concentration of glucose (72 mM, 72 h). **(f)** Secreted amount of HMGB1 from the MSC spheroids that were formed with MSCs treated with different concentration of SPIO@Chitosan-GL according to different glucose concentration. Data were expressed as mean ± s.e.m (n = 5). **P < 0.01 and ***P < 0.001 versus MSCs were treated with 0 μg/ml of SPIO@Chitosan-GL at 75 mM glucose concentration. **(g)** Intracellular amount of HMGB1 in the MSC spheroids that were formed with MSCs treated with different concentration of SPIO@Chitosan-GL according to different glucose concentration. Data were expressed as mean ± s.e.m (n = 5). **P < 0.01 and ***P < 0.001 versus MSCs were treated with 5 μg/ml of SPIO@Chitosan-GL at 75 mM glucose concentration. **(h)** Serum concentration of complement factor C3a after intraportal transplantation of MSC single cells or spheroids. Blood samples were collected at 0 or 30 min after intraportal transplantation of MSC spheroids. Data were expressed as mean ± s.e.m (n = 3). **P < 0.01 and ***P < 0.001.

SPIO@Chitosan-GL was observed in MSC spheroids (GFP-stained area), which is explained by the formation of MSC spheroids after SPIO@Chitosan-GL uptake in single MSCs and stably localizing and functioning at the implanted site for a long period of time.

2.7. Effect of SPIO@Chitosan-GL nanoparticle in MSC spheroid under the cellular damage

Therefore, we optimized the concentration of SPIO@Chitosan-GL through evaluating responsiveness to the magnetic field (Fig. 6a). The MSC spheroids labeled with 5 μg/ml of SPIO@Chitosan-GL still responded well to the magnetic field of strength of 2000 G given at a distance of 5 cm from the dish (their reaction velocity at magnetic field: ~345 μm/s) (Fig. 6b and c). Then, we optimized the concentration of SPIO@Chitosan-GL using *in vitro T2*-weighted MRI phantom analysis (Fig. 6d). The MSC spheroids labeled with 5 μg/ml of SPIO@Chitosan-GL were clearly visualized in agar gel phantom without image blurring. After that, to evaluate whether the internalized SPIO@Chitosan-GL could attenuate the secretion of HMGB1, *i.e.*, inflammatory protein, in MSC spheroids, we measured the amount of HMGB1 on MSC spheroids after cellular damage with high concentration of glucose (Fig. 6e). HMGB1 content was normally maintained in the cell at low glucose concentration (2 mM), meaning that the internalized SPIO@Chitosan-GL did not affect the release of HMGB1 (Fig. 6f). When MSC spheroids were damaged with high glucose (75 mM), HMGB1 was significantly released into culture medium. However, SPIO@Chitosan-GL-labeled MSC spheroids significantly attenuated HMGB1 release. To confirm low release of HMGB1, we measured the intracellular HMGB1 content of the MSC spheroids. The intracellular HMGB1 content was significantly reduced by cell damage with high glucose in the case of no treatment of SPIO@Chitosan-GL (Fig. 6g). Interestingly, SPIO@Chitosan-GL-labeled MSC spheroids had significantly higher intracellular HMGB1 content at cellular damage with high glucose. These results correlated with the ability of SPIO@Chitosan-GL (5 μg/ml) to attenuate HMGB1 release in islets (see Fig. 3f). Therefore, internalization of SPIO@Chitosan-GL could significantly regulate the secretion of HMGB1 regardless of cell type.

On the other hand, C3a, one of the proteins formed by cleavage of complement factor, is an inflammation-inducing molecule [36]. In addition, C3a could bind to RAGE (receptor for advanced glycosylation end-products) with high affinity [37]. Also it could form a complex with CpG oligonucleotides to enhance release of interferon-α (IFN-α) cytokine from leukocytes [38]. The concentration of C3a can be increased in the bloodstream after islet and MSCs are infused through the portal vein of liver, because HMGB1 released from the damaged therapeutic cells induces conversion of C3 to C3a as a part of IBMIR. Internalization of SPIO@Chitosan-GL into MSC spheroids can reduce C3 to C3a conversion through attenuated release of HMGB1 by damaged MSC spheroids, thereby lowering serum C3a levels and reducing the instant blood mediated inflammatory reaction (IBMIR) [39,40].

The serum concentration of C3a was measured 30 min after the transplantation of MSC spheroids, considering that the IBMIR occurs immediately after intraportal infusion of therapeutic cells. In this regard, islet transplantation is a process in which a massive destruction of majority of transplanted islets occurs during the first few days by IBMIR, hypoxia, and metabolic stress. Surviving islets can achieve engraftment after ~14 days of revascularization process [41]. We agree that C3a levels in immediate posttransplant period of co-transplantation of islets and MSC spheroids would be informative for documentation of reduction in IBMIR. However, the serum C3a levels were not measured during the co-transplantation experiments for a reason. Because there was a critical trade-off between the benefit of measuring serum C3a levels by blood sampling of small animals (C57BL/6J mice) and major stress induction in experiments requiring the survival of animals for >4 weeks. Stress during the early posttransplant period of islet transplantation is a major perturbing factor in islet graft function. This is because transplanted islets are most vulnerable to stress during the early post-transplant period before engraftment with revascularization. In presence of major stress, the glycemic outcome of islet transplantation is confounded, as hyperglycemia could be more severe in recipient animals that are more vulnerable to stress.

As a result, the intrahepatically transplanted MSC single cells or MSC spheroids without SPIO@Chitosan-GL highly induced the serum concentration of C3a even though their cell number was lower (Fig. 6h). However, the serum concentration of C3a was significantly low at transplantation of SPIO@Chitosan-GL-labeled MSC spheroids although their cell number was higher those in other groups. Furthermore, C3a is known to contain a binding domain with high affinity for glycyrrhizin [42]. Therefore, it is expected that the result is not only due to the attenuation of IBMIR by reduced release of HMGB1, but also that the conformational change of C3 after binding with glycyrrhizin may be additionally involved in the anti-inflammatory effect in vivo.

2.8. Therapeutic effect of SPIO@Chitosan-GL-labeled pancreatic islets and MSC after intrahepatic co-transplantation with magnetic guidance

Next, we co-transplanted allogenic mouse-derived pancreatic islets and allogenic mouse-derived MSC spheroids into the liver of diabetic mouse under magnetic guidance to evaluate therapeutic effect of SPIO@Chitosan-GL in allotransplantation condition, which is relevant setting with current clinical allotransplantation (Fig. 7a). To this end, SPIO@Chitosan-GL was separately treated or not in both cells, and then intrahepatically infused in the streptozotocin (STZ)-induced diabetic mouse. In general, it is known that islet architecture is fundamentally different among various species [43]. However, taken together with *in vitro* results, SPIO@Chitosan-GL nanoparticles could be well internalized in both rat-derived and mouse-derived islets. After allotransplantation, the blood glucose outcomes in the diabetic recipients were monitored with a short 5-days cyclosporine A (CsA) regimen, which was suitable for assessing post-transplant loss of pre-transplantation cell grafts. Transplantation of unlabeled pancreatic islets alone did not completely reverse STZ-induced diabetes, even during CsA injection (black circle, Fig. 7b). In addition, co-transplantation of unlabeled pancreatic islets and unlabeled MSC spheroids reversed STZ-induced diabetes for 13 days (triangle, Fig. 7b), demonstrating the cytoprotective effect of the stem cells. The survival time (16–18 days) of SPIO@Chitosan-GL-labeled islets alone were very similar to transplantation of SPIO@Chitosan-GL-labeled islets with unlabeled MSC spheroids (white circle and inverted triangle, Fig. 7b), suggesting that the cytoprotective effect of MSC spheroid was limited. These results might be attributed to the release of HMGB1 protein (see Figs. 3f and 6f). In general, HMGB1 is known to play a crucial role in the early loss of transplanted islets in a diabetic mice model, which is highly correlated to immune rejection [39]. This is because pancreatic islets contained abundant HMGB1, which was released into the circulation soon after islet transplantation into the liver. Mechanistically, HMGB1 stimulates hepatic mononuclear cells (MNCs), which upregulate CD40 expression and increases IL-12 production by dendritic cells (DCs). It then leads to NKT cell activation and NKT cell-dependent increased IFN-γ production by Gr-1^{+}CD11b^{+} cells. Therefore, inhibition of HMGB1 secretion from islet cell is significant to prevent early islet graft loss mediated by immune rejection. In this regard, GL, which exhibits high affinity for HMGB1 in SPIO@Chitosan-GL-labeled islets, is expected to inhibit HMGB1 secretion and successfully attenuate the immune rejection response that occurs during islet transplantation. On the other hand, co-transplantation of SPIO@Chitosan-GL-labeled pancreatic islets and SPIO@Chitosan-GL-labeled MSC spheroids significantly lowered the mean blood glucose levels in the diabetic recipients to within 200 mg/dl for 30 days after transplantation (black square, Fig. 7b).

When we compared the % proportion of HMGB1-, CD68^{-}, and CD3-stained area to insulin-stained area in the islet grafts of the two groups with co-transplantation of islets and MSC spheroids (SPIO@Chitosan-

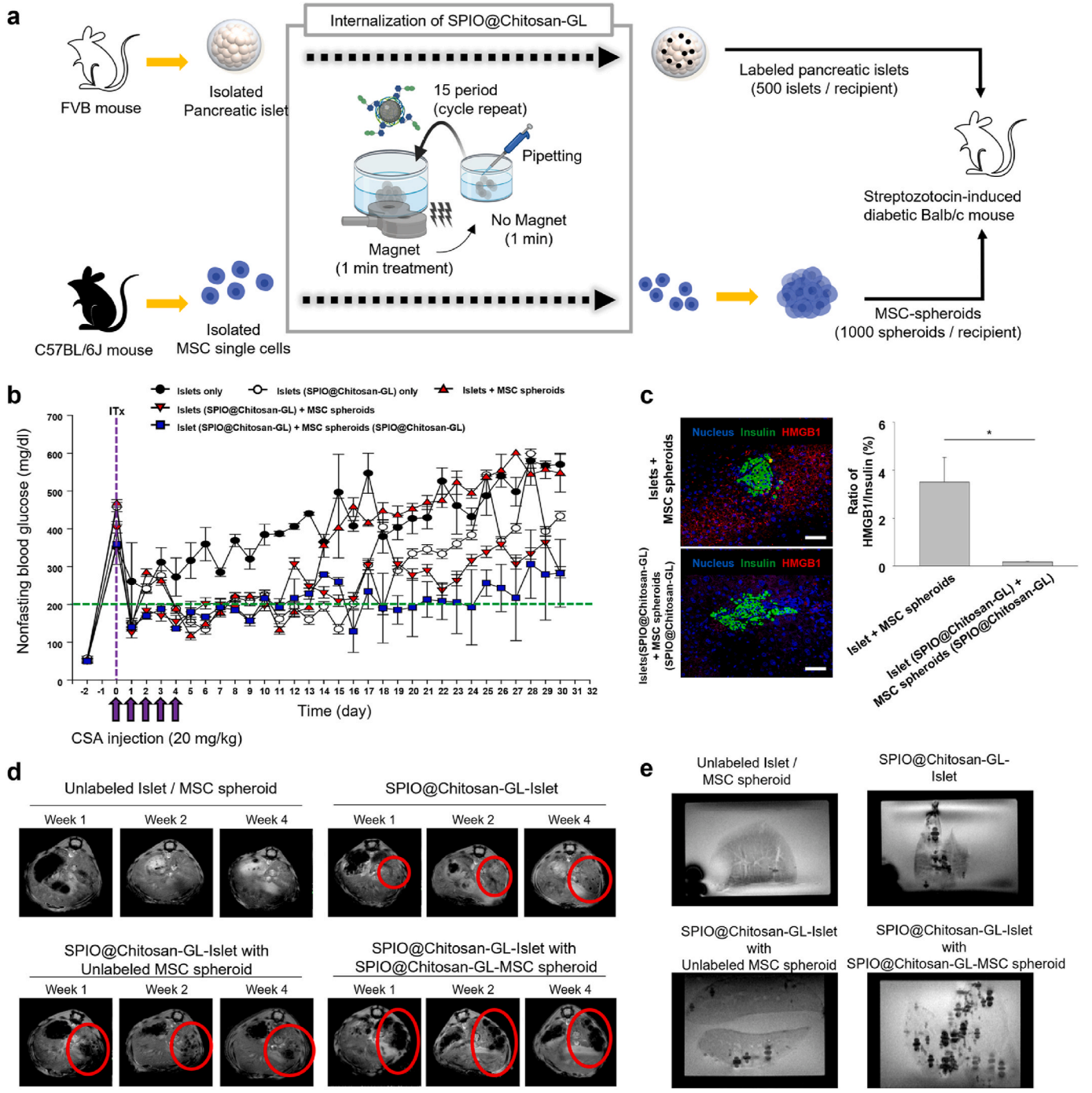

Fig. 7. Therapeutic effect of SPIO@Chitosan-GL-labeled pancreatic islets and MSC spheroids intraportally co-transplanted with magnetic guidance. (**a**) Allo-transplantation of pancreatic islets and MSC spheroids after SPIO@Chitosan-GL internalization. (**b**) Nonfasting blood glucose level of the diabetic recipients after intraportal co-transplantation with magnetic guidance. Data were expressed as mean ± s.e.m (n = 5). ITx: intraportal transplantation at day 0. Arrow: immuno-suppressant cyclosporin A (CsA, 20 mg/kg) injection. Green dash line: standard dotted line for judging diabetes treatment (200 mg/dl). (**c**) Immunofluorescence image and HMGB1/insulin (%) ratio in the islet grafts of the two groups with co-transplantation of islets and MSC spheroids (SPIO@Chitosan-GL-islets with SPIO@Chitosan-GL MSC spheroids group vs. unlabeled islets with unlabeled MSC-spheroids group). Data were expressed as mean ± standard deviation. Scale bar: 100 μm. (**d**) *In vivo T2*-weighted MR images of the diabetic recipients after intraportal co-transplantation with magnetic guidance. Red circle: the detected islets and MSC spheroids. (**e**) *In vitro T2*-weighted MR images of the sectioned median lobe of liver organ after intraportal co-transplantation with magnetic guidance. Black spots: the detected islets and MSC spheroids. (For interpretation of the references to color in this figure legend, the reader is referred to the Web version of this article.)

GL-islets with SPIO@Chitosan-GL MSC spheroids group and unlabeled islets with unlabeled MSC-spheroids group), the SPIO@Chitosan-GL-islets with SPIO@Chitosan-GL MSC spheroids group showed lower proportion of HMGB1-, CD68^{-}, and CD3-stained area to insulin-stained area in the islet grafts (Fig. 7c and Fig. S14). We also explored if the SPIO@Chitosan-GL MSC spheroids are present in the recipient liver four weeks after co-transplantation of SPIO@Chitosan-GL pancreatic islets with SPIO@Chitosan-GL MSC spheroids. As a result, it was confirmed that the grafted area on the slide was stained with Prussian blue (black-dashed circles). Markers for pancreatic islet (anti-insulin antibody, red-

dashed circles) and MSC spheroids (anti-GFP and anti-stem cell antigen-1 (Sca1) antibody, blue-dashed circles) were also stained adjacent to the iron stained-site (Fig. S15).

Given that the durable euglycemia was achieved only when both the SPIO@Chitosan-GL-islets and SPIO@Chitosan-GL MSC spheroids were transplanted (Fig. 7b). These findings may indicate that the profound difference in the glycemic levels between the two groups was attributable to the inflammatory state of the islet grafts, probably mediated by the reduced release of HMGB1 by of SPIO@Chitosan-GL uptake in both cell types.

In vivo MRI of the diabetic recipients transplanted with SPIO@Chitosan-GL-labeled pancreatic islets or SPIO@Chitosan-GL-labeled MSC spheroids showed hypointense spots successfully localized in the median lobe of the liver for 4 weeks post-transplantation (Fig. 7d), indicating that both cells could be well co-localized in the intended location by magnetic guidance. In addition, SPIO@Chitosan-GL-labeled pancreatic islets or/and SPIO@Chitosan-GL-labeled MSC spheroids were strongly detected when the dissected median lobe was sectioned and analyzed with *in vitro* MRI phantom (Fig. 7e). Meanwhile, to ascertain whether the recipients' diabetic reversal is truly attributable to the transplanted SPIO@Chitosan-GL-labeled pancreatic islets, we partially hepatectomized the median lobe in which SPIO@Chitosan-GL-labeled pancreatic islets were selectively localized by magnetic guidance. The blood glucose levels of partially hepatectomized recipients were immediately hyperglycemic (Fig. S16), indicating that the transplanted pancreatic islets were successfully localized in the median lobe of the liver and were responsible for the normoglycemia. It was also demonstrated that the localized islets could be safely removed without whole hepatectomy in the event of an inflammatory reaction in the liver. Next, we thoroughly explored if there was remnant hepatic infarction in the four weeks post-transplantation liver tissues and found that there was no evidence of hepatic infarction in transplantation sites in all animals (Fig. S17). Given that islet transplantation has been accepted as a safe procedure unless portal thrombosis occurs, we sought to ensure that there is no evidence of safety issue in the 4-week liver tissues.

3. Conclusion

Collectively, SPIO@Chitosan-GL nanoparticle would be useful for co-transplantation of islets with adjuvant therapeutic cells such as mesenchymal stem cells (MSCs), which can be facilitated by co-localization of islets and adjuvant therapeutic cells [34]. Given that most MSCs are substantially damaged in the early stage of their engraftment and IBMIR [33], intracellular delivery of GL as SPIO@Chitosan-GL to islets and MSCs would result in better immunological protection. Both treated cells offer a higher probability of synergistic effects by paracrine mechanism. Given that both SPIO and GL has been clinically used without safety issues [14,15], we speculated that our approach could offer an important breakthrough for the widespread clinical use of pancreatic islet transplantation and potentially any cell therapy with MSCs.

4. Materials and methods

4.1. Conjugation of glycyrrhizin-glycol chitosan (Chitosan-GL)

To synthesis glycyrrhizin-glycol chitosan conjugate (Chitosan-GL), glycyrrhizin ammonium salt (GL; 411.5 mg; Sigma-Aldrich, St. Louis, Missouri, USA) was dissolved in 10 ml of carbonate buffer solution (CBS; pH 9.5) at 4 °C. Sodium periodate (214 mg; Sigma-Aldrich) was also dissolved in 10 ml of deionized water, which was slowly dropped into the as-prepared glycyrrhizin solution and reacted for 90 min at 4 °C, thereby preparing the oxidized glycyrrhizin (oGL). Separately, glycol chitosan (205.7 mg; Wako pure chemical industries, Osaka, Japan) was dissolved in 10 ml of CBS (pH 9.5) at 4 °C, which was also further dropped into the oGL solution and gently shake at 4 °C for 24 h. To stably become the glycyrrhizin-glycol chitosan (Chitosan-GL) conjugate, cyanoborohybride (15 μL; Sigma-Aldrich) was further dropped into the solution and reacted for 24 h. After that, the solution was purified with dialysis membrane (MWCO 3500–5000 Da; membrane filtration products, USA) in CBS (pH 9.5) for 48 h and then further dialyzed in deionized water for 72 h. The dialysis buffer solution was newly replaced at each time. Then, the purified solution was replaced into 50-ml tube and frozen with liquid nitrogen. It was freeze-dried for 3 days to be lyophilized. Finally, the powder form of Chitosan-GL was obtained. The link between GL and glycol chitosan was confirmed by Fourier-transform infrared (FT-IR) spectroscopy (Nicolet™ iS™50 FR-IR Spectrometer; Thermo scientific, Waltham, MA, USA) and ^{1}H NMR (500 MHz NMR Avance-500, Bruker, Germany).

4.2. Preparation of SPIO@Chitosan-GL nanoparticle

To synthesize superparamagnetic iron oxide (SPIO) nanoparticle, iron (II) chloride tetra hydrate (0.28 g, Sigma-Aldrich) and iron(III) chloride hexahydrate (0.56 g, Sigma-Aldrich) were dissolved at 30 ml of deionized water in 3-neck round bottom flask. Rubber stoppers were put on the flask and nitrogen gas was injected for 30 min to remove oxygen in the flask. After nitrogen gas injection was stopped, ammonium hydroxide (8 ml, Sigma-Aldrich) was dropped in the flask with syringe and gently stirred for 30 min under the nitrogen gas purge to make precipitation of the SPIO nanoparticle. The solution in the flask was transferred to a 100-ml beaker that was put on a neodymium circular magnet (5-cm in diameter, 5000 G). When the black-colored SPIO nanoparticles were precipitated at the bottom by the magnet, the supernatant was removed. Then 20 ml of deionized water was added in the beaker and vigorously mixed with pipetting. This washing step was repeated twice more.

To coat superparamagnetic iron oxide (SPIO) nanoparticle with Chitosan-GL, the lyophilized Chitosan-GL (100 mg) was dissolved in 10 ml of deionized water. If it was not completely dissolved well, 5–10 μL of acetic acid was added. The fully dissolved as-prepared SPIO nanoparticle solution was poured into the Chitosan-GL solution and stirred at 80 °C for 2 h. And then, the solution was sonicated ice condition for 1 h with a specific condition (39% amplification; On time: 2sec, Off time: 2 s, Total time: 1 h condition). To remove the uncoated SPIO nanoparticles, the solution was put on the neodymium magnet for 5 min. Then the supernatant was collected and centrifuged for 10 min. After that, the supernatant was filtered with 0.8-μm pore size and then further filtered with 0.45-μm pore size. The final solution of Chitosan-GL-coated SPIO, *i.e.*, SPIO@Chitosan-GL, nanoparticles was stored at 4 °C and left at room temperature before use. The size of SPIO@Chitosan-GL was measured by using transmission electron microscope (TEM, Joel, Peabody, MA 01960, USA). The surface potential and size of SPIO@Chitosan-GL nanoparticle was measured using a zeta sizer (Nano ZS, Melvern, UK).

5. Animal purchase and study approval

Male Sprague Dawley (SD) rat, C57BL/6J mice, or FVB mice of seven-week-old were purchased from Nara-Bio Company, Seoul, Korea. Animals were controlled in Specific Pathogen-Free (SPF) condition in accordance with the provisions of the Institutional Animal Care and Use Committee (IACUC) at Hanyang University. Feed was given once a day and an automated watering system was used. The experimental protocol was approved by IACUC (No. 2018-0205A) and conformed to the guidelines for the Care and Use of Laboratory Animals.

5.1. Internalization of SPIO@Chitosan-GL into isolated pancreatic islets

To isolate pancreatic islets, 10 ml of collagenase P solution (1 mg/ml in Hanks' balanced salt solution; Roche, Basel, Switzerland) was intraductally injected into the common duct of pancreas organ in male Sprague Dawley (SD) rat, C57BL/6J mice or FVB mice. The expended

pancreases organ was surgically and incubated for enzymatic digestion in water bath (37 °C) for 15 min. After adding the complete medium, purification of isolated islets was carried out by using discontinuous Histopaque (Sigma) and centrifugation. The purified islets in the layer of Histopaque was collected washed two times. To recover the purified islets, they were cultured for 24 h in RPMI-1640 (Invirogen, Carlsbad, CA, USA) which contains 10% fetal bovine serum (Sigma) and 1% antibiotics for further experiments. The isolated islets were cultured in a cell culture incubator (37 °C, 5% CO_2) before use.

For internalization of SPIO@Chitosan-GL into isolated pancreatic islets, pancreatic islets were seeded in 35-mm dish and treated with the dissolved SPIO@Chitosan-GL (109.5 μg/ml). To prevent the precipitation of SPIO@Chitosan-GL to the bottom of dish, the culture medium was gently pipetted for 1 min. Then the dish was quickly moved under the magnetic field of the neodymium circular magnet (2000 G, 5-cm in diameter) and maintained for 1 min. These serial steps were defined as a 1-cycle procedure. To optimize internalization of SPIO@Chitosan-GL, various concentration of SPIO@Chitosan-GL was treated to pancreatic islets with different cycle numbers and reaction time: (a) simple treatment without magnet, (b) static magnetic field (SMF), (c) static magnetic field with gentle pipetting (SMF-P), and (d) frequency alternating magnetic field (F-AMF). After that, the internalized amount of SPIO@Chitosan-GL was quantified with iron colorimetric assay kit (K390; Biovision, Milpitas, USA). In addition, the viability of SPIO@Chitosan-GL-labeled MSCs was measured by using Cell counting kit-8 (CCK-8; Dojindo Molecular Technologies, Rockville, MD, USA).

5.2. Preparation of murine pancreatic mesenchymal stem cells (MSC)

Murine pancreatic MSCs were isolated from male green fluorescent protein-transgenic (GFP-Tg) and wild-type C57BL/6J mice aged 10–12 weeks, as describe elsewhere [34]. Pancreatic cells left at the bottom after islet isolation by density gradient separation were washed in PBS and cultured with α-MEM medium supplemented with 10% FBS and 1% penicillin/streptomycin. Medium was changed after 24–48h to remove nonadherent cells. When cultures reached confluence, cells were trypsinized and subcultured. In the present study, we used MSCs at passage 3. The cell surface marker pattern of the MSCs was confirmed flow cytometry, as describe elsewhere [34]. The Institutional Animal Care and Use Committee of Samsung Biomedical Research Institute approved all animal experimental protocols in this study.

5.3. Internalization of SPIO@Chitosan-GL into murine pancreatic mesenchymal stem cells (MSC)

For internalization of SPIO@Chitosan-GL into murine pancreatic mesenchymal stem cell (MSC), the detached MSC was seeded on 35-mm culture dish (5×10^5 cells/dish) and cultured for overnight. Next day, they were treated with various concentration of SPIO@Chitosan-GL solution. Total volume of culture medium in dish was set to 3 ml for all groups. Immediately, SPIO@Chitosan-GL treated dish was put under the magnetic field of neodymium circular magnet (2000 G, 5-cm in diameter) for 1 min and the quickly put off the magnetic field for 1 min. This cycle was totally repeated 8 times. After that, the internalized amount of SPIO@Chitosan-GL was quantified with iron colorimetric assay kit. In addition, the viability of SPIO@Chitosan-GL-labeled MSCs was measured by using CyQUANT LDH assay kit (C20300; TermoFisher Scientific, Waltham, MA, USA).

5.4. Spheroid formation of SPIO@Chitosan-GL-labeled MSC

For spheroid formation of SPIO@Chitosan-GL-labeled MSCs, they were collected and diluted to be 5×10^4 cell/ml. Then, 20 μl of medium having the cells (1000 cell/20 μl) was mildly dropped on the surface of 150-mm dish cover. The dish covers with droplets were carefully inverted and put onto the 150-mm dish that was filled with 15 ml of culture medium to prevent evaporation of the droplets during cultivation. After cultivation for 3 days, the newly formed MSC spheroids were collected and cultured. The morphology of the SPIO@Chitosan-GL-labeled MSC spheroids was observed with microscope.

5.5. Cell viability assay of SPIO@Chitosan-GL-labeled islets or MSC spheroids

For cell viability assays, SPIO@Chitosan-GL-labeled islet and MSCs were seeded in 96-well plates for each well and cells were treated with the culture medium containing EZ-Cytox (Itsbio Inc., Seoul, Korea) at 37 °C and 5% CO_2 for 4 h. After that, the viability of cells which labeled with various concentration of SPIO@Chitosan-GL (0, 2.5, 5, 10, 20, 45 μg/ml) and long culture (1, 3, 5, 7 days) was measured by measuring the absorbance at 450 nm wavelength.

5.6. Moving velocity of SPIO@Chitosan-GL-labeled islets or MSC spheroids under the magnetic field in vitro

For evaluation of moving velocity of SPIO@Chitosan-GL-labeled pancreatic islets or MSC spheroids, they were gathered on the bottom of 35-mm culture dish. Then magnetic field with neodymium magnet was applied at the 5 cm distance from the gathered islets or spheroids to induce their mobility toward the magnet. During mobility of the islets or spheroids, running distance between start position and moved position at every second was measured with Image-J software. Finally, the moving velocity of the islets or spheroid was calculated.

5.7. Inhibition of HMGB1 release from SPIO@Chitosan-GL-labeled islet or MSC spheroid in vitro

To evaluate whether the internalized SPIO@Chitosan-GL nanoparticles could attenuate the HMGB1 release from the isolated islets and MSC spheroids, the cellular damage against islets and MSCs were occurred by using streptozotocin (STZ) or high concentration of glucose. In the case of cellular damage to rat pancreatic islets, unlabeled or SPIO@Chitosan-GL-labeled islets (50 IEQ/ml/well in 48-well plate) were treated with 1.5 mM STZ and reacted for 2 h. After that, the cultured medium was collected for Rat HMGB1 ELISA kit (NBP3-06661; Novus Biologicals, Centennial, USA). All steps were followed according to the procedure of manufacturer. On the other hand, in the case of cellular damage to murine pancreatic MSC spheroids, unlabeled or SPIO@Chitosan-GL-labeled MSC spheroids were treated with 75 mM glucose and reacted for 72 h. After that, the culture medium was collected for human HMGB1 ELISA kit (NPB2-62766; Novus Biologicals). In both cases, the size variant of pancreatic islets and the MSC spheroids were compensated with the amount of DNA contents measured by using DNA quantitation kit (DNAQF-1KT; Sigma-Aldrich).

5.8. Intraportal transplantation of SPIO@Chitosan-GL-leveled pancreatic islets and MSC spheroids into the lobe of liver in diabetic mouse

For transplantation of pancreatic islets and/or MSC spheroids, STZ-induced diabetic C57BL/6J mice were anesthetized with injection of Zoletil/Rumpun mixture solution (mixing ratio 4:1; 100 μl). Then pancreatic islets (500 IEQ/mouse) or MSC spheroids (1000 spheroids/mouse) were collected in 20 μl of saline, which was transferred to a surgical butterfly needle and connected with Hamilton syringe. After that, the butterfly needle containing islets or MSC spheroids was smoothly poked into the portal vein of the mice and they were slowly infused. During infusion, the magnetic field with neodymium magnet was simultaneously applied to selectively localize the islets or MSC spheroids into the median lobe of the liver. As control group, instead of magnetic field, a hemostatic clip band was put on the site of injection to mechanically guide them into the median lobe of the liver. After transplantation, the blood glucose level of the mouse was continuously

monitored to confirm whether the SPIO@Chitosan-GL-labeled islets and/or MSC spheroids could cure the diabetic mellitus.

5.9. Partial hepatectomy for removal of intrahepatically transplanted cells

To confirm whether the blood glucose level to the mouse was regulated by the transplanted SPIO@Chitosan-GL-labeled islets, the median lobe of the liver was partially hepatectomized at day 8 after transplantation. After partial hepatectomy, the blood glucose level of the mouse was further continuously monitored to evaluate the increment of blood glucose level. At the end of experiment, all mice were sacrificed, and the whole liver organ was detached and dissociated with each lobe of liver (total 7 lobes) that were fixed with 4% formalin solution for 3 days. And then, the fixed lobes were paraffin-blocked, sectioned, and stained with the hematoxylin and eosin (HE) dye.

5.10. Magnetic resonance imaging (MRI) of SPIO@Chitosan-GL-labeled islets or MSC spheroids in vivo and in vitro

In vivo magnetic resonance imaging (MRI) was performed to confirm the effect of magnetic guidance during infusion of SPIO@Chitosan-GL-labeled islets or MSC spheroids. After transplantation of them, the mice were anesthetized and scanned with *T2*-weighted imaging using by the 7.0 T MR scanner (Bruker-Biospin, Ettlingen, Germany). The detailed parameters and procedures in the MRI experiments were described elsewhere [44]. Briefly, anesthetized mice were restrained in the prone position. Coronal *T2*-weighted MR images were acquired using a FLASH (Fast low angle shot) sequence with the following acquisition parameters: repetition time of 231 msec; echo time of 8.0 msec; field of view (FOV) of 27.0 × 27.0 mm; matrix size of 270.0 × 270.0; flip angle of 30.0°; signal averaging number of 10; and 16 total slices with a slice thickness of 1.0 mm and no inter-slice gaps. SPIO@Chitosan-GL-labeled pancreatic islets appeared as hypointense signals on *T2*-weighted MR images.

In vitro MRI was confirmed to evaluate whether the transplanted SPIO@Chitosan-GL-labeled islets and MSC spheroids were mainly located at the median of the liver. To this end, the dissociated with each lobe of liver (total 7 lobes) that were fixed with 4% formalin solution for 3 days. Then they were put in 150-mm Petri dish and 1% agarose gel solution was brimmingly poured to get rid of the noisy caused by oxygen. All petri dishes were moved into the 7.0 T MR scanner to perform *T2*-weighted MR imaging.

5.11. Immunofluorescence of transplanted SPIO@Chitosan-GL-labeled pancreatic islets

To evaluate transplanted SPIO@Chitosan-GL-labeled pancreatic islets, the sectioned tissue slides were fixed with primary anti-insulin antibody or anti-HMGB1 antibody (dilution 1:200; Invitrogen, Waltham, MA, USA) simultaneously with 20% goat serum for overnight at 4 °C. And next day, secondary AlexaFluor 488 goat anti-rabbit (dilution 1: 1000, green color fluorescence; Invitrogen) were dropped into all slides for 1 h at room temperature without light. Then the slides were washed with PBS and counter-stained with fluorescent DAPI dye (Sigma-Aldrich). The immunostained tissue slides were observed through a fluorescence microscope. On the other hand, to verify the existence of SPIO@Chitosan-GL in the transplanted islets, the sectioned tissue slides were first stained with iron stain kit (ab150674; Prussian blue stain; Abcam) for 10 min, which was intended for use in the detection ferric ion in the slide.

5.12. Image analysis of islet or MSC spheroid grafts and evaluation of graft morphology

To detect transplanted SPIO@Chitosan-GL-labeled pancreatic islets in liver, the liver tissue slides were deparaffinized and were blocked with phosphate-buffered saline (PBS) containing 5% normal goat serum and 0.1% Tween-20 for 1 h. For paraffin-embedded sections, antigen retrieval was performed in 10 Mm citrate buffer at pH 6.0 for 5 min, 3 times. After blocking, the tissue slides were stained with primary antibodies HMGB1 clone 951,420 (R&D systems, Mab16901, Minneapolis, USA), recombinant anti-insulin antibody (abcam, ab181547, Cambridge, UK), anti-CD3 antibody (abcam, ab5690, Cambridge, UK), and CD68 (abcam, ab955, Cambridge, UK) overnight at 4 °C. The next day, the slides were washed three times with PBST and then incubated with secondary antibodies as follows: Goat anti-rabbit IgG H&L (Alexa Fluor 594, 1:1000) (abcam, ab150080, Cambridge, UK), goat anti-rabbit IgG H&L (Alexa fluor 488, 1:1000) (abcam, ab150077, Cambridge, UK), and donkey anti-rat IgG H&L (Alexa 594) (abcam, ab150156, Cambridge, UK). Cell nuclei were visualized using DAPI (1:10,000 dilutions of 14.3 μM stock) (Invitrogen, D1306, Massachusetts, USA). The stained slides were taken by using confocal microscope Zeiss LSM 780 and the percentage of markers positive areas were analyzed by image J.

The total liver was sectioned stained with primary antibody anti-GFP (1:500, Cell Signaling, mAb#2955) and anti-Sca-1 (1:500, Cell signaling, mAb#4336) and secondary antibody Goat anti-mouse IgG (H + L) HRP (1:1000, invitrogen #31430) and then the slides were visualized with diaminobenzidine (DAB) reagent kit (Dako, K-5007) after counter stained using Mayer's hematoxylin. The total liver tissue (4 μm interval section) areas were captured and measured with Aperio ScanScope® AT2 Turbo (Aperio Technologies, Inc., Vista, CA) and the ratio of islet to whole liver area were quantified using Aperio ImageScope 12.0.

6. Statistics

All data were expressed as mean ± S.E.M, and *t*-test was used to verify the significance between experimental group and control group (Sigma stat Software, CA, USA). The *t*-test results were statistically significant only when the p value was 0.05 or less.

Data and materials availability

All data are available tin the main text or the supplementary materials.

Credit author statement

The manuscript was written through contributions of all authors. All authors have given approval to the final version of the manuscript. ‡These authors contributed equally as First Author. **These authors contributed equally as Corresponding Author. S.B.J.: Conceptualization, Methodology, Investigation, Writing- Original Draft. S.M.J.: Validation, Data Curation, Writing- Original Draft. S.J.L.: Conceptualization, Methodology, Investigation, Writing- Original Draft. Y.Y.J.: Methodology, Validation, Data Curation. H.S.K.: Methodology, Investigation, Visualization. S.H.: Methodology, Investigation. H.S.L.: Methodology, Investigation. J.H.K.: Supervision, Project administration, Funding acquisition. D.Y.L.: Conceptualization, Methodology, Investigation, Writing- Original Draft, Writing - Review & Editing, Supervision, Project administration, Funding acquisition.

Funding

This research was supported by the Korea Health Technology R&D Project through the Korea Health Industry Development Institute funded by the Ministry of Health & Welfare (HI18C0453); the National Research Foundation funded by the MSIT (NRF-2020R1A2C3005834, NRF-2022R1A4A1030421, NRF-2020R1A2C1004590), Republic of Korea.

Declaration of competing interest

The authors declare the following financial interests/personal relationships which may be considered as potential competing interests: Prof. Dong Yun Lee is a founder, CEO and major shareholder of Elixir Pharmatech Inc., which focuses on the use of the system described in this work for different disease states, including inflammatory bowel disease. Other authors declare no known competing financial interest.

Data availability

Data will be made available on request.

Appendix A. Supplementary data

Supplementary data to this article can be found online at https://doi.org/10.1016/j.biomaterials.2022.121679.

References

[1] F.H. Gage, Cell therapy, Nature 392 (6679 Suppl) (1998) 18–24.
[2] S. Lablanche, S. Borot, A. Wojtusciszyn, F. Bayle, R. Tetaz, L. Badet, C. Thivolet, E. Morelon, L. Frimat, A. Penfornis, L. Kessler, C. Brault, C. Colin, I. Tauveron, D. Bosco, T. Berney, P.Y. Benhamou, G. Network, Five-Year metabolic, functional, and safety results of patients with type 1 diabetes transplanted with allogenic islets within the Swiss-French GRAGIL network, Diabetes Care 38 (9) (2015) 1714–1722.
[3] B.J. Hering, W.R. Clarke, N.D. Bridges, T.L. Eggerman, R. Alejandro, M.D. Bellin, K. Chaloner, C.W. Czarniecki, J.S. Goldstein, L.G. Hunsicker, D.B. Kaufman, O. Korsgren, C.P. Larsen, X. Luo, J.F. Markmann, A. Naji, J. Oberholzer, A. M. Posselt, M.R. Rickels, C. Ricordi, M.A. Robien, P.A. Senior, A.M. Shapiro, P. G. Stock, N.A. Turgeon, C. Clinical, Islet transplantation, phase 3 trial of transplantation of human islets in type 1 diabetes complicated by severe hypoglycemia, Diabetes Care 39 (7) (2016) 1230–1240.
[4] M. Qi, K. Kinzer, K.K. Danielson, J. Martellotto, B. Barbaro, Y. Wang, J.T. Bui, R. C. Gaba, G. Knuttinen, R. Garcia-Roca, I. Tzvetanov, A. Heitman, M. Davis, J. J. McGarrigle, E. Benedetti, J. Oberholzer, Five-year follow-up of patients with type 1 diabetes transplanted with allogeneic islets: the UIC experience, Acta Diabetol. 51 (5) (2014) 833–843.
[5] G.H. Goodwin, C. Sanders, E.W. Johns, A new group of chromatin-associated proteins with a high content of acidic and basic amino acids, Eur. J. Biochem. 38 (1) (1973) 14–19.
[6] T. Itoh, S. Iwahashi, M.A. Kanak, M. Shimoda, M. Takita, D. Chujo, Y. Tamura, A. M. Rahman, W.Y. Chung, N. Onaca, P.T. Coates, A.R. Dennison, B. Naziruddin, M. F. Levy, S. Matsumoto, Elevation of high-mobility group box 1 after clinical autologous islet transplantation and its inverse correlation with outcomes, Cell Transplant. 23 (2) (2014) 153–165.
[7] Y. Cheng, J. Xiong, Q. Chen, J. Xia, Y. Zhang, X. Yang, K. Tao, S. Zhang, S. He, Hypoxia/reoxygenation-induced HMGB1 translocation and release promotes islet proinflammatory cytokine production and early islet graft failure through TLRs signaling, Biochim. Biophys. Acta, Mol. Basis Dis. 1863 (2) (2017) 354–364.
[8] N. Matsuoka, T. Itoh, H. Watarai, E. Sekine-Kondo, N. Nagata, K. Okamoto, T. Mera, H. Yamamoto, S. Yamada, I. Maruyama, M. Taniguchi, Y. Yasunami, High-mobility group box 1 is involved in the initial events of early loss of transplanted islets in mice, J. Clin. Invest. 120 (3) (2010) 735–743.
[9] L. Mollica, F. De Marchis, A. Spitaleri, C. Dallacosta, D. Pennacchini, M. Zamai, A. Agresti, L. Trisciuoglio, G. Musco, M.E. Bianchi, Glycyrrhizin binds to high-mobility group box 1 protein and inhibits its cytokine activities, Chem. Biol. 14 (4) (2007) 431–441.
[10] L. Rackova, V. Jancinova, M. Petrikova, K. Drabikova, R. Nosal, M. Stefek, D. Kostalova, N. Pronayova, M. Kovacova, Mechanism of anti-inflammatory action of liquorice extract and glycyrrhizin, Nat. Prod. Res. 21 (14) (2007) 1234–1241.
[11] K.R. Kim, C.K. Jeong, K.K. Park, J.H. Choi, J.H. Park, S.S. Lim, W.Y. Chung, Anti-inflammatory effects of licorice and roasted licorice extracts on TPA-induced acute inflammation and collagen-induced arthritis in mice, J. Biomed. Biotechnol. 2010 (2010), 709378.
[12] Y. Fu, E. Zhou, Z. Wei, D. Liang, W. Wang, T. Wang, M. Guo, N. Zhang, Z. Yang, Glycyrrhizin inhibits the inflammatory response in mouse mammary epithelial cells and a mouse mastitis model, FEBS J. 281 (11) (2014) 2543–2557.
[13] D.L. Ni, C.A. Ferreira, T.E. Barnhart, V. Quach, B. Yu, D.W. Jiang, W.J. Wei, H. S. Liu, J.W. Engle, P. Hu, W.B. Cai, Magnetic targeting of nanotheranostics enhances cerenkov radiation-induced photodynamic therapy, J. Am. Chem. Soc. 140 (44) (2018) 14971–14979.
[14] C. Toso, J.P. Vallee, P. Morel, F. Ris, S. Demuylder-Mischler, M. Lepetit-Coiffe, N. Marangon, F. Saudek, A.M. James Shapiro, D. Bosco, T. Berney, Clinical magnetic resonance imaging of pancreatic islet grafts after iron nanoparticle labeling, Am. J. Transplant. : official j. Am. Soc. Transplant. Am. Soc. Transplant Surg. 8 (3) (2008) 701–706.
[15] F. Saudek, D. Jirak, P. Girman, V. Herynek, M. Dezortova, J. Kriz, J. Peregrin, Z. Berkova, K. Zacharovova, M. Hajek, Magnetic resonance imaging of pancreatic islets transplanted into the liver in humans, Transplantation 90 (12) (2010) 1602–1606.
[16] J. Pan, Y.Y. Xu, Q.S. Wu, P. Hu, J.L. Shi, Mild magnetic hyperthermia-activated innate immunity for liver cancer therapy, J. Am. Chem. Soc. 143 (21) (2021) 8116–8128.
[17] J. Chen, N. Huang, B. Ma, M.F. Maitz, J. Wang, J. Li, Q. Li, Y. Zhao, K. Xiong, X. Liu, Guidance of stem cells to a target destination in vivo by magnetic nanoparticles in a magnetic field, ACS Appl. Mater. Interfaces 5 (13) (2013) 5976–5985.
[18] L.H.A. Silva, M.C. Silva, J.B. Vieira, E.C.D. Lima, R.C. Silva, D.J. Weiss, M. M. Morales, F.F. Cruz, P.R.M. Rocco, Magnetic targeting increases mesenchymal stromal cell retention in lungs and enhances beneficial effects on pulmonary damage in experimental silicosis, Stem Cells Transl Med 9 (10) (2020) 1244–1256.
[19] F. Johansson, M. Jonsson, K. Alm, M. Kanje, Cell guidance by magnetic nanowires, Exp. Cell Res. 316 (5) (2010) 688–694.
[20] N. Nitin, L.E. LaConte, O. Zurkiya, X. Hu, G. Bao, Functionalization and peptide-based delivery of magnetic nanoparticles as an intracellular MRI contrast agent, J. Biol. Inorg. Chem. 9 (6) (2004) 706–712.
[21] B. Dubertret, P. Skourides, D.J. Norris, V. Noireaux, A.H. Brivanlou, A. Libchaber, In vivo imaging of quantum dots encapsulated in phospholipid micelles, Science 298 (5599) (2002) 1759–1762.
[22] E. Amstad, S. Zurcher, A. Mashaghi, J.Y. Wong, M. Textor, E. Reimhult, Surface functionalization of single superparamagnetic iron oxide nanoparticles for targeted magnetic resonance imaging, Small 5 (11) (2009) 1334–1342.
[23] D.W. Chakeres, F. de Vocht, Static magnetic field effects on human subjects related to magnetic resonance imaging systems, Prog. Biophys. Mol. Biol. 87 (2–3) (2005) 255–265.
[24] J.M. Theysohn, O. Kraff, K. Eilers, D. Andrade, M. Gerwig, D. Timmann, F. Schmitt, M.E. Ladd, S.C. Ladd, A.K. Bitz, Vestibular effects of a 7 Tesla MRI examination compared to 1.5 T and 0 T in healthy volunteers, PLoS One 9 (3) (2014), e92104.
[25] C. Heilmaier, J.M. Theysohn, S. Maderwald, O. Kraff, M.E. Ladd, S.C. Ladd, A large-scale study on subjective perception of discomfort during 7 and 1.5 T MRI examinations, Bioelectromagnetics 32 (8) (2011) 610–619.
[26] M. Goto, J. Holgersson, M. Kumagai-Braesch, O. Korsgren, The ADP/ATP ratio: a novel predictive assay for quality assessment of isolated pancreatic islets, Am. J. Transplant. : official j. Am. Soc. Transplant. Am. Soc. Transplant Surg. 6 (10) (2006) 2483–2487.
[27] K.K. Papas, C.K. Colton, A. Qipo, H. Wu, R.A. Nelson, B.J. Hering, G.C. Weir, M. Koulmanda, Prediction of marginal mass required for successful islet transplantation, J. Invest. Surg. 23 (1) (2010) 28–34.
[28] S.J. He, J. Cheng, X. Feng, Y. Yu, L. Tian, Q. Huang, The dual role and therapeutic potential of high-mobility group box 1 in cancer, Oncotarget 8 (38) (2017) 64534–64550.
[29] N. Lee, H. Kim, S.H. Choi, M. Park, D. Kim, H.C. Kim, Y. Choi, S. Lin, B.H. Kim, H. S. Jung, H. Kim, K.S. Park, W.K. Moon, T. Hyeon, Magnetosome-like ferrimagnetic iron oxide nanocubes for highly sensitive MRI of single cells and transplanted pancreatic islets, P Natl Acad Sci USA 108 (7) (2011) 2662–2667.
[30] T. Ito, S. Itakura, I. Todorov, J. Rawson, S. Asari, J. Shintaku, I. Nair, K. Ferreri, F. Kandeel, Y. Mullen, Mesenchymal stem cell and islet co-transplantation promotes graft revascularization and function, Transplantation 89 (12) (2010) 1438–1445.
[31] K.S. Park, Y.S. Kim, J.H. Kim, B. Choi, S.H. Kim, A.H. Tan, M.S. Lee, M.K. Lee, C. H. Kwon, J.W. Joh, S.J. Kim, K.W. Kim, Trophic molecules derived from human mesenchymal stem cells enhance survival, function, and angiogenesis of isolated islets after transplantation, Transplantation 89 (5) (2010) 509–517.
[32] D.J. Borg, M. Weigelt, C. Wilhelm, M. Gerlach, M. Bickle, S. Speier, E. Bonifacio, A. Hommel, Mesenchymal stromal cells improve transplanted islet survival and islet function in a syngeneic mouse model, Diabetologia 57 (3) (2014) 522–531.
[33] G. Moll, I. Rasmusson-Duprez, L. von Bahr, A.M. Connolly-Andersen, G. Elgue, L. Funke, O.A. Hamad, H. Lonnies, P.U. Magnusson, J. Sanchez, Y. Teramura, K. Nilsson-Ekdahl, O. Ringden, O. Korsgren, B. Nilsson, K. Le Blanc, Are therapeutic human mesenchymal stromal cells compatible with human blood? Stem Cell. 30 (7) (2012) 1565–1574.
[34] B.J. Oh, S.M. Jin, Y. Hwang, J.M. Choi, H.S. Lee, G. Kim, G. Kim, H.J. Park, P. Kim, S.J. Kim, J.H. Kim, Highly angiogenic, nonthrombogenic bone marrow mononuclear cell-derived spheroids in intraportal islet transplantation, Diabetes 67 (3) (2018) 473–485.
[35] C. Mennan, S. Brown, H. McCarthy, E. Mavrogonatou, D. Kletsas, J. Garcia, B. Balain, J. Richardson, S. Roberts, Mesenchymal stromal cells derived from whole human umbilical cord exhibit similar properties to those derived from Wharton's jelly and bone marrow, Febs Open Bio 6 (11) (2016) 1054–1066.
[36] L.G. Coulthard, T.M. Woodruff, Is the complement activation product C3a a proinflammatory molecule? Re-evaluating the evidence and the myth, J. Immunol. 194 (8) (2015) 3542–3548.
[37] J. Xie, J.D. Mendez, V. Mendez-Valenzuela, M.M. Aguilar-Hernandez, Cellular signalling of the receptor for advanced glycation end products (RAGE), Cell. Signal. 25 (11) (2013) 2185–2197.
[38] B.H. Ruan, X. Li, A.R. Winkler, K.M. Cunningham, J. Kuai, R.M. Greco, K.H. Nocka, L.J. Fitz, J.F. Wright, D.D. Pittman, X.Y. Tan, J.E. Paulsen, L.L. Lin, D.G. Winkler, Complement C3a, CpG oligos, and DNA/C3a complex stimulate IFN-alpha production in a receptor for advanced glycation end product-dependent manner, J. Immunol. 185 (7) (2010) 4213–4222.
[39] N. Matsuoka, T. Itoh, H. Watarai, E. Sekine-Kondo, N. Nagata, K. Kamoto, T. Mera, H. Yamamoto, S. Yamada, I. Maruyama, M. Taniguchi, Y. Yasunami, High-mobility group box 1 is involved in the initial events of early loss of transplanted islets in mice, J. Clin. Invest. 120 (3) (2010) 735–743.

[40] T. Itoh, S. Iwahashi, M.A. Kanak, M. Shimoda, M. Takita, D. Chujo, Y. Tamura, A. M. Rahman, W.Y. Chung, N. Onaca, P.T.H. Coates, A.R. Dennison, B. Naziruddin, M.F. Levy, S. Matsumoto, Elevation of high-mobility group box 1 after clinical autologous islet transplantation and its inverse correlation with outcomes, Cell Transplant. 23 (2) (2014) 153–165.
[41] X.Y. Li, Q. Meng, L. Zhang, The fate of allogeneic pancreatic islets following intraportal transplantation: challenges and solutions, J Immunol Res 2018 (2018).
[42] F. Kawakami, Y. Shimoyama, K. Ohtsuki, Characterization of complement C3 as a glycyrrhizin (GL)-binding protein and the phosphorylation of C3alpha by CK-2, which is potently inhibited by GL and glycyrrhetinic acid in vitro, J. Biochem. 133 (2) (2003) 231–237.
[43] A. Kim, K. Miller, J. Jo, G. Kilimnik, P. Wojcik, M. Hara, Islet architecture: a comparative study, Islets 1 (2) (2009) 129–136.
[44] S.M. Jin, H.S. Lee, M.R. Haque, H.N. Kim, H.J. Kim, B.J. Oh, K.W. Lee, G. Kim, H. S. Kim, D.Y. Lee, J.B. Park, S.J. Kim, Y. Byun, J.H. Kim, Multi-layer surface modification of pancreatic islets for magnetic resonance imaging using ferumoxytol, Biomaterials 214 (2019), 119224.